DOI:
10.1016/j.celrep.2020.108451

Document Version
Peer reviewed version

HIV infection of latent tuberculosis subjects skews a balanced Mtb-specific Th17 response to a proinflammatory Th17 profile that is independent of cellular viral load

Srabanti Rakshit[1], Nitin Hingankar[1], Shuba Varshini Alampalli[1], Vasista Adiga[1], Bharath K. Sundararaj[1], Pravat Nalini Sahoo[1], Greg Finak[2], Anto Jesuraj UK J[3], Chirag Dhar[3], George D' Souza[3], Rashmi Govind Virkar[4], Manisha Ghate[4], Madhuri Thakar[4], Ramesh Paranjape[4], Stephen C. De Rosa[2], Tom HM Ottenhoff[5], Annapurna Vyakarnam[1,6]

[1]Laboratory of Immunology of HIV-TB co-infection, Centre for Infectious Disease Research, Indian Institute of Science, Bangalore, India.

[2]Vaccine and Infectious Disease Division, Fred Hutchinson Cancer Research Center, Seattle, WA, United States of America.

[3]Department of Infectious Diseases & Department of Pulmonary Medicine, St John's Research Institute, Bangalore, India.

[4]National Aids Research Institute, Bhosari, Pune, Maharashtra, India.

[5]Department of Infectious Diseases, Leiden University Medical Center, Leiden, Netherlands.

[6]Peter Gorer Department of Immunobiology, School of Immunology and Microbial Sciences, Faculty of Life Sciences & Medicine, Guy's Hospital, King's College London, London SE1 9RT, UK.

***Correspondence to:**

Dr. Annapurna Vyakarnam;

Centre for Infectious Disease Research

Indian Institute of Science; Bangalore 560012 and

Department of Immunobiology, School of Immunology & Microbial Sciences,

King's College London

Tel: 0091-80-2360-4348 (land line, India)/091-9945385960 (mobile, India)

E-mail: anna.vyakarnam@kcl.ac.uk annapurnavyakarnam@gmail.com

Conflict of Interest Statement

The authors declare that the research was conducted in the absence of any commercial or financial relationships that could be construed as a potential conflict of interest.

SUMMARY

HIV is a major risk factor for tuberculosis (TB) in latent TB infected (LTBI) subjects. This study was designed to determine if HIV infection of LTBI subjects compromises a balanced Mtb-specific Th17 response, of recognised importance in anti-TB immunity. Comparative analysis of Mtb and CMV-specific $CD4^+$ T-cell responses using multiparameter flow cytometry demonstrates a selective and marked dampening of the Mtb-, but not CMV-specific response in LTBI subjects chronically infected with HIV. A significant loss of Mtb-specific $CD4^+$ T-cell effectors expressing total IFN-γ, IL-2, TNF-α, MIP-1β and IL-17F as well as polyfunctional cells comprising upto 256 cell subsets was noted. Additionally, there was marked skewing of the Mtb-specific Th17 response with preservation of specific proinflammatory IFN-γ/IL-17 and significant loss of anti-inflammatory IL-10/IL-17 double positive effectors. This switch in Th17 profile restored by ART treatment was noted in chronic HIV-infected LTBI progressors but not LTBI long-term non-progressors. The HIV-driven impairment of Mtb-specific effectors cannot be attributed to selective HIV infection as cell-associated HIV DNA and HIV RNA revealed equivalent viral burden in Mtb-, CMV- and HIV-specific $CD4^+$ T effectors. We therefore propose that beyond HIV-induced loss of Mtb-specific $CD4^+$ T-cells, the associated dysregulation of Mtb-specific T effector cell homeostasis can potentially enhance the onset of TB in LTBI subjects.

INTRODUCTION

AIDS and tuberculosis (TB) are among the top 10 leading causes of death worldwide. The interaction between the two causative pathogens, HIV and *Mycobacterium tuberculosis* (Mtb) exacerbates disease pathology and substantially contributes to this high incidence of mortality (**Diedrich and Flynn, 2011)**. In 2018, globally 38 million people were estimated to be HIV$^+$, of which 862,000 were diagnosed as TB-positive. Furthermore, TB is the leading cause of death among people with HIV accounting for one-third of HIV-related deaths i.e. 251,000 out of 770,000 people died from HIV-associated TB in 2018 (**WHO TB Report 2019; UNAIDS Report 2019**). Healthy subjects with latent TB infection (LTBI) are reportedly identified by the QuantiFERON® TB Gold In-tube Interferon Gamma Release Assay (IGRA) and commonly referred to as either LTBI or IGRA$^+$ (henceforth referred to as IGRA$^+$) (**Auguste et al., 2017**). Although the majority of IGRA$^+$ subjects remain asymptomatic over their lifetime, 5-15% progress to active disease manifested either as pulmonary TB (PTB) in the lung or extrapulmonary TB (EPTB) in the lymph nodes, pleura, abdomen and other organs (**Lin and Flynn, 2018**). Chronic HIV infection enhances the risk of TB reactivation by >20-fold and annual incidence by 5-15% (**Pawlowski et al., 2012; Bell and Noursadeghi, 2018)** that is reduced by 67% in ART-treated IGRA$^+$ subjects (**Lawn et al., 2015**). On the other hand, increased incidence of TB in IGRA$^+$ HIV-infected long-term non-progressors (LTNP), who are defined as remaining asymptomatic for at least seven years following infection with preserved CD4 T-cell counts despite being viremic and not on ART (**Ciccone et al., 2011**), has not been reported. Hence, deciphering the mechanisms by which HIV infection predisposes IGRA$^+$ subjects to TB is an area of significant scientific and global health interest.

Insight on immune mechanisms by which HIV may drive TB disease have emerged from both human studies and from non-human primate (NHP) models of HIV-TB coinfection. Reactivation of TB in NHP, is not likely solely governed by reduced CD4$^+$ T-cell counts induced by HIV infection but depends on other immune factors, including macrophage disruption (**Kuroda et al., 2018**) and absence of granzyme-positive CD8$^+$ T-cells (**Foreman et al., 2016**). Human studies, on the other hand, highlight both HIV-induced CD4$^+$ T-cell depletion and functional changes of Mtb-specific CD4$^+$ T-cells to be major factors by which HIV drives TB incidence (**Douek et al., 2003; Geldmacher et al., 2010; Okoye and Picker, 2013; Esmail et al., 2018; Murray et al., 2018; Amelio et al., 2019**). Understanding the precise functional changes that HIV infection of humans induces in the Mtb-specific T-cell response is therefore important. Several phenotypic

and functional studies highlight selective vulnerability of Mtb-specific $CD4^+$ T-cells to HIV infection. Effector memory $CD4^+$ T-cells that express the HIV entry receptor CCR5, are dramatically depleted in the gut which serve as a major *in vivo* reservoir of infection (**Yang et al., 2012**). Importantly, $CD4^+$ memory T-cells primed to recognize Mtb and HIV antigens express elevated levels of HIV entry coreceptor, CCR5, and conversely low in the anti-HIV chemokine, MIP-1β, which binds CCR5 and blocks HIV entry; these cells are consequently highly susceptible to HIV infection, whereas memory cells specific for CMV, an opportunistic pathogen that emerges late in HIV infection, are poorly infected linked to high MIP-1β expression and lower CCR5 expression (**Geldmacher et al., 2010; Geldmacher et al., 2012; Bronke et al., 2005**). Moreover, Mtb-specific $CD4^+$ T-cells display an early differentiated phenotype with enhanced proliferation potential due to higher IL-2 production making them more permissive to HIV infection than the terminally differentiated CMV-specific $CD4^+$ T-cells (**Ahmed et al., 2016**). Additionally, cytokine imbalance and loss of polyfunctional Mtb-specific $CD4^+$ T-cells is also associated with HIV-infected IGRA status (**Amelio et al., 2019; Day et al., 2008; Riou et al., 2016**; **Day et al., 2017**).

Within the CD4 compartment, a major focus is to understand how HIV alters the Mtb-specific Th17 responses based on substantial recent evidence highlighting $CD4^+$ Th17 cells, which otherwise are important in maintaining gut mucosa integrity, to play crucial roles in protective immunity against HIV and Mtb infection (**Esmail et al., 2018**). Th17 cells exhibit considerable heterogeneity and plasticity as they can differentiate into distinct subsets in the presence of specific cytokine milieu. Naive $CD4^+$ T-cells cultured in the presence of TGF-β and IL-6 differentiate into regulatory and protective Th17 that co-express of IL-17 and IL-10, while the additional presence of IL-1β and/or IL-23 steers them toward the pro-inflammatory and pathogenic Th17 cells that co-express of IL-17 and IFN-γ (**Mercer et al., 2014**). Moreover, Mtb-specific memory cells in IGRA+ subjects are mostly contained within the $CXCR3^+CCR6^+$ CD4+ T-cell subset that express both IFN-γ and IL-17 and represent the pathogenic phenotype (**Acosta-Rodriguez et al., 2007**). Further, $CCR4^+CCR6^+$ Th17 and $CXCR3^+CCR6^+$ (Th1/Th17) cells that express the HIV coreceptors CCR5 and CXCR4 and secrete low levels of MIP-1β are highly susceptible to *in vitro* infection by R5 and X4 HIV viruses (**Elhed et al., 2010; Gosselin et al., 2010).** Additionally, these Th17 subsets also exhibit gut- and lymph node-homing potential that might relate to their significant depletion in the gastrointestinal tract of chronic HIV-infected individuals **(Bixler and Mattapallil, 2013**), but not in HIV-infected LTNP (**Ciccone et al., 2011; Caetano et al., 2020**).

Data from our laboratory has provided the first evidence of the potential importance of a balanced Mtb-specific Th17 response in TB immunity. We demonstrated the presence of Mtb-specific regulatory or anti-inflammatory IL-17$^+$ cells that co-expressed IL-10 in IGRA$^+$ subjects, whilst subjects with TB disease showed significant loss of this subset whilst preserving Mtb-specific proinflammatory IL-17$^+$ cells that co-expressed IFN-γ (**Rakshit et al., 2017**). Additionally, sterile granulomas in a TB NHP model were associated with increased T-cells producing both IL-10 and IL-17 (**Gideon et al., 2015**). Importantly, protective immunity to Mtb infection induced by BCG vaccination in a live challenge NHP model was associated with IL-10 and Mtb-specific Th17 CD4$^+$ T-cells (**Dijkman et al., 2019**). In our recent study involving young human adults, we showed that BCG revaccination has the potential to enhance Mtb-specific IL-17$^+$ cells that co-expressed IL-10 but not IL-17$^+$ cells that co-expressed IFN-γ (**Rakshit et al., 2019**). The aim of this study was therefore to investigate the impact of HIV infection on the nature of the Mtb-specific Th17 response. We hypothesized that HIV infection of IGRA$^+$ subjects would alter the balance of Mtb-specific Th17 pro- vs anti-inflammatory IL-17$^+$ cells, skewing the response to a proinflammatory phenotype previously noted in subjects with TB disease (**Rakshit et al., 2017**), thereby potentially predisposing IGRA$^+$ subjects to TB disease progression. We provide evidence in support of our hypothesis through a comparative analysis of immune profiles combined with HIV load analyses in CD4$^+$ T-cells specific for Mtb vs. CMV in IGRA$^+$ subjects with progressive HIV disease vs. HIV$^+$IGRA$^+$ long-term non-progressors (LTNP) and subjects with TB with and without chronic HIV infection before and after ART or ATT treatment.

RESULTS

HIV infection significantly reduces the absolute numbers of total Mtb-specific CD4$^+$ T-cells in IGRA$^+$ individuals

HIV Infection leads to the functional impairment of Mtb-Specific CD4$^+$ and CD8$^+$ T-cell responses (**Amelio et al., 2019**); however, the precise mechanisms by which HIV hampers the Mtb-specific CD4$^+$ T-cell response is poorly understood To address this issue, we first compared the absolute numbers of Mtb-specific CD4$^+$ T-cells in subjects from the following four clinical groups: HIV$^+$IGRA$^+$ versus HIV$^-$IGRA$^+$ and HIV$^+$IGRA$^-$ versus HIV$^-$IGRA$^-$, with all HIV$^+$ subjects displaying significantly lower absolute CD4 T-cell counts than the HIV-uninfected counterpart group (**see Table 1**). Representative FACS plots depicting the complete stepwise gating strategy to identify functional subsets is shown in Figure S1. Comparison of HIV$^-$IGRA$^+$ versus HIV$^+$IGRA$^+$ subjects (green versus red scatter plots) would assess the impact of chronic HIV infection on Mtb-specific responses of IGRA$^+$ subjects, whilst a comparison of HIV$^-$IGRA$^-$ versus HIV$^+$IGRA$^-$ subjects (brown versus blue scatter plots) would determine the impact of chronic HIV infection independent of IGRA status (**Figures 1A and 1B)**. We measured the expression of 6 key effector cytokines, namely IFN-γ, IL-2, MIP-1β, TNF-α, IL-10 and IL-17F in response to the *Mtb* ESAT6/CFP10 fusion protein referred to as EC- and to a pool of 4 *Mtb* DosR latency antigens (Rv1733c, Rv1737c, Rv2029 and Rv2628), referred to as LT Ag in CD4$^+$ Tcells. These antigens were selected based on previous studies showing responses to the LT Ag in particular to clearly distinguish asymptomatic IGRA$^+$ subjects from those with active TB disease (**Rakshit et al., 2017; Coppola and Ottenhoff, 2018)**. To determine if HIV infection impacted recall responses, we compared the Mtb-specific response with that of CMV. Unlike TB, which is evident at all stages of HIV infection, CMV emerges late in HIV infection as an opportunistic pathogen concomitant with profound CD4$^+$ T-cell loss. Mitogen driven (PHA) responses were measured to evaluate the impact on global T-cell responses, irrespective of cell specificity. Representative flow cytometry plots depict effector cytokine expression by CD4$^+$ T-cells to different antigenic stimuli relative to unstimulated negative control (**Figure S2)**.

Figure S3 show the total frequencies of cytokine positive CD4$^+$ T-cells enumerated and in Figures 1A and 1B, the same data is represented as absolute CD4$^+$ numbers corrected for individual donors' CD4$^+$ T-cell counts, thereby enabling an accurate estimation of specific CD4$^+$ T-cell changes across subjects with wide

variations in their circulating $CD4^+$ T-cell numbers (**see Table 1**). We record significant reduction in all cytokine subsets specific for both EC and LT Ag in HIV^+IGRA^+ (red) versus HIV^-IGRA^+ (green), with the exception of IL-10 (**Figure 1A)**. Consistent with lower or minimal Mtb antigenic burden in $IGRA^-$ compared to $IGRA^+$ subjects (**Carpenter et al., 2015**), the $IGRA^-$ groups, HIV^+ (blue) and HIV^- (brown) on the whole had lower absolute numbers of these Mtb-specific $CD4^+$ T-cells compared to their $IGRA^+$ counterparts (red and green), (**Figures 1A and 1B**). Except for TNF-α, the downward trend noticed in the absolute numbers of most cytokines to EC stimulation did not reach statistical significance; neither were there any appreciable differences in absolute numbers of cytokines to LT Ag stimulation in HIV^+IGRA^- compared to HIV^-IGRA^- subjects (**Figure 1B**). In keeping with previous data (**Geldmacher et al., 2010**), a marked 10-fold reduction in MIP-1β was noted in Mtb-specific cells from the $IGRA^+$ group, whereas an increase in the absolute numbers of MIP-$1\beta^+$ CMV-specific $CD4^+$ T-cells was observed in $IGRA^-$ subjects following HIV infection (**Figures 1A and 1B**). With the exception of MIP-1β, all other effector cytokine responses measured to CMV and PHA stimulation were similar across all subjects tested, providing strong evidence that HIV infection had the potential to selectively impair Mtb-specific recall responses in $IGRA^+$ subjects (**Figures 1A and 1B**). These changes observed in absolute numbers of effector cytokine-positive $CD4^+$ T-cells concurred with changes in cytokine frequencies (see **Figure S3**). We also evaluated the impact of HIV infection on Mtb-specific $CD8^+$ T-cell responses. Figure S4 shows no significant differences in the total frequencies of Mtb-specific $CD8^+$ T-cells expressing IFN-γ and TNF-α in HIV-uninfected versus -infected subjects. However, absolute numbers of EC-specific $CD8^+$ T-cells expressing IFN-γ in HIV^+IGRA^+ and the LT Ag-specific $CD8^+$ T-cells expressing TNF-α in HIV^+IGRA^- were significantly enhanced compared to their respective HIV^- counterparts (**Figure S4**). Our CD8 data is broadly consistent with other human studies showing no significant changes in frequencies of EC-specific $CD8^+IFN\text{-}\gamma^+$ T-cells in HIV-infected individuals irrespective of IGRA status or CD4 T-cell counts (**Murray et al. 2018, Kalokhe AS et al. 2015**) with the increase in absolute number of cytokine-positive $CD8^+$ T-cells in HIV^+IGRA^+ subjects (**Figure S4**), likely due to the recognised HIV-infection induced increase in blood CD8 T-cell counts (**Chiacchio et al. 2018**). The absolute numbers of CMV-specific total $IFN\text{-}\gamma^+$ and $TNF\text{-}\alpha^+$ $CD4^+$ and $CD8^+$ T-cells, for all study participants has been provided in Figure S5. Consistent with previous reports showing CMV recall responses to be well preserved (**Chiacchio et al. 2018; Murray et al. 2018**), we demonstrate a high proportion of CMV-specific $CD4^+$ (100%) and $CD8^+$ (80-90%) T-cell responders in the subjects recruited to our study (**Figure S5)**.

HIV infection reduces the polyfunctional Mtb-specific response of IGRA$^+$ subjects

Mtb-specific, central memory polyfunctional responses are an important hallmark of IGRA$^+$ subjects (**Rakshit et al., 2017; Arroyo et al., 2016**) and can be impaired by HIV infection (**Day et al., 2017; Diedrich and Flynn, 2011**). We therefore evaluated the differences in polyfunctional CD4$^+$ T-cell responses between HIV$^-$IGRA$^+$ versus HIV$^+$IGRA$^+$ subjects using a panel of 8 key effector cytokines (IFN-γ, IL-2, TNF-α, MIP-1β, IL-10, IL-17A, IL-17F and IL-22). Polyfunctionality was determined by analysing all 256 different combinations of these 8 cytokines stratified using the Boolean gating strategy in FlowJo and employing COMbinatorial Polyfunctionality Analysis of Antigen-Specific T-cell Subsets (COMPASS) (**Lin et al., 2015**), an advanced bioinformatics software to derive polyfunctional scores (PFS) (**Figure 2A**). Differences in PFS between groups were estimated through a linear model fit to the PFS for each antigen (see STAR Methods). After multiple testing adjustments, significant reduction was observed in the CD4$^+$ T-cell polyfunctional response to LT Ag stimulation and a trend for EC in HIV$^+$IGRA$^+$ compared to that of HIV$^-$IGRA$^+$ subjects (**Figure 2A**). Further, consistent with the total cytokine data in **Figure 1**, the polyfunctional response in IGRA$^-$ subjects, was significantly lower than that of IGRA$^+$ subjects. In-depth visualisation of immune subsets simultaneously expressing one, two, three, four and five combinations of cytokines are illustrated as heatmaps in **Figure S6**, with a detailed explanation included in the supplementary file (results section). The polyfunctional CD4$^+$ T-cell response was further probed by analysis of the above data (**Figure 2A**) in Simplified Presentation of Incredibly Complex Evaluations (SPICE) (**Roederer et al., 2011**). Using this software, the global cytokine profile induced in IGRA$^+$ subjects to EC and LT Ag stimulation represented as pie charts in Figure 2B were functionally similar but each of these responses were profoundly impacted by HIV infection (**Figure 2B**). This analysis clearly demonstrates the striking loss of single MIP-1β$^+$ cells (shown as blue arcs) and the EC-specific double-positive TNF-α$^+$MIP-1β$^+$ subset but an increase of single TNF-α$^+$ cells (shown as purple arcs) in all HIV$^+$ subjects independent of IGRA status (**Figure 2B**). In addition, this analysis revealed that HIV reduces many combinations of 2$^+$, 3$^+$, 4$^+$ and 5$^+$ cells whilst preserving single-positive IFN-γ, IL-2, IL-17F and IL-10 cells in HIV$^+$IGRA$^+$ and HIV$^+$IGRA$^-$ compared to HIV$^-$IGRA$^+$ subjects, thereby indicating an overall impairment of polyfunctional responses in HIV$^+$ subjects (**Figure 2B**). Taken together, our data demonstrate that CD4$^+$ T-cell polyfunctional responses are markedly impaired in HIV$^+$IGRA$^+$ subjects, with LT Ag-specific cells being particularly impacted.

HIV infection skews the balanced Mtb-specific Th17 response in IGRA$^+$ subjects

Previously we have shown that a balanced Mtb-specific Th17 response comprising both IL-17$^+$IFN-γ$^+$ pro-inflammatory and IL-17$^+$IL-10$^+$ anti-inflammatory effectors to be a hallmark of HIV$^-$IGRA$^+$ individuals (**Rakshit et al., 2017**). Therefore, we sought to evaluate the status of the Th17 response in IGRA$^+$ subjects following HIV infection. Using COMPASS, we conducted a detailed analysis of the probability of EC and LT Ag-specific CD4$^+$ Th17 cells for each subject averaged across selected functional profiles for either IFN-γ or IL-10 together with all combinations of IL-17A, IL-17F and IL-22 **(Figure 3A)**. HIV$^+$IGRA$^+$ and HIV$^+$IGRA$^-$ subjects had significantly fewer LT Ag-specific regulatory CD4$^+$ Th17 subsets co-expressing IL-10 with IL-17A/IL-17F/IL-22, whereas the reduction of these subsets was not statistically significant for EC-specific cells, indicating that the LT Ag-specific Th17 response was more significantly impacted by HIV infection compared to the EC response (**Figure 3A**).

To further interrogate the above data, we used SPICE to identify the precise Mtb-specific Th17 subsets that were altered by HIV infection by separately enumerating the absolute numbers of three combinations of double-positive pro-inflammatory (IFN-γ$^+$IL-17A$^+$; IFN-γ$^+$IL-17F$^+$ and IFN-γ$^+$IL-22$^+$) and three combinations of double-positive anti-inflammatory or regulatory (IL-10$^+$IL-17A$^+$; IL-10$^+$IL-17F$^+$ and IL-10$^+$IL-22$^+$) Th17 cell subsets (see methods), with representative FACS profiles shown in **Figure S7**. In Figure 3B, we demonstrate the impact of HIV infection on each of these six subsets in IGRA$^+$ subjects. We highlight the following salient points: (i) Absolute CD4$^+$ T-cell numbers of all three EC- and LT Ag-specific regulatory Th17 subsets co-expressing IL-10, which form a minor but distinct viable cell population as confirmed by back gating analysis (**Figure S8**), is significantly lower in HIV$^+$IGRA$^+$ versus HIV$^-$IGRA$^+$ subjects (**Figure 3B**). (ii) Although IFN-γ$^+$IL-17A$^+$ and IFN-γ$^+$IL-22$^+$ subsets were significantly reduced by HIV infection noticeably to LT Ag but not to EC stimulation, the absolute numbers of these pro-inflammatory subsets were relatively higher than the IL-10$^+$ regulatory subsets, suggesting that regulatory subsets are impacted to a greater extent upon HIV infection (**Figure 3B**).

Next, we conducted a detailed analysis of HIV infection on Mtb-specific Th17 subsets across seven different clinical groups where Th17 cells were grouped into pro-inflammatory (IFN-γ expression with either IL-17A/IL-17F or IL-22) or anti-inflammatory (IL-10 expression with either IL-17A/IL-17F or IL-22) subsets. In addition, we probed the impact of HIV infection on IFN-γ $^+$IL-10$^+$ cells, another anti-inflammatory regulatory subset (referred to as Tr1 cells) reportedly expanded in chronic infections, including TB (**Trinchieri., 2001**).

Figure 3C shows these three subset comparisons in IGRA$^+$ and IGRA$^-$ HIV$^+$ progressors; IGRA$^+$ HIV$^+$ long term non-progressors; HIV$^+$ subjects with TB and HIV uninfected IGRA$^+$, IGRA$^-$ and TB$^+$ subjects serving as controls. Absolute numbers of cytokine positive cells corrected for multiple comparisons across these seven clinical groups is shown in **Figure 3C**, with salient observations as follows: (i) Most HIV$^-$IGRA$^-$ subjects (brown) lacked EC and LT Ag-specific pro-inflammatory IFN-γ$^+$ Th17 cells but had low absolute numbers (less than 0.1%) of IL-10$^+$ regulatory Th17 cells. (ii) Notably, HIV infection of IGRA$^-$ subjects enhanced the pro-inflammatory Th17 subset (blue). (iii) Compared to HIV$^-$IGRA$^-$ subjects, HIV$^-$IGRA$^+$ subjects (green) had a greater LT Ag- and EC-specific Th17 response (0.1% and greater), with HIV infection inducing dramatic loss of regulatory IL-10$^+$ Th17 subsets (red). (iv) A comparison of IGRA$^+$ HIV$^+$ progressors who had low CD4 T-cell counts with those of IGRA$^+$ HIV$^+$ long term non-progressors (LTNP) with preserved CD4 T-cell counts showed that LTNPs have mainly regulatory Th17 subsets with low proportion of pro-inflammatory IFN-γ$^+$ Th17 subsets (magenta). (v) The data also highlights that HIV negative subjects with TB disease (black) to have the highest numbers of pro-inflammatory IFN-γ$^+$ Th17 cells compared to any other group with few regulatory IL-10$^+$IL-17$^+$ cells, however HIV infection in TB$^+$ subjects leads to a further decrease in both regulatory as well as pro-inflammatory Th17 subsets (dark grey). (vi) Furthermore, we demonstrate that IFN-γ$^+$IL-10$^+$ cells are present in HIV$^-$IGRA$^+$ and HIV$^+$IGRA$^+$LTNP subjects but low in HIV$^+$IGRA$^+$ and HIV$^+$TB$^+$ groups. Taken together these data provide strong evidence that HIV infection significantly impacts the balance between pro- and anti-inflammatory Mtb-specific Th17 subsets with significant dysregulation of the Mtb-specific regulatory Th17 cells co-expressing IL-10 following chronic HIV infection of IGRA$^+$ subjects.

Anti-retroviral (ART) and anti-TB (ATT) therapies enhance Mtb-specific total cytokine effector responses

ART and ATT have been shown to increase the absolute numbers of Mtb-specific CD4$^+$ T-cells in HIV-IGRA$^+$ subjects (**Chiacchio et al., 2018**). We sought to investigate whether ART and ATT can restore Mtb-specific cytokine responses impacted by HIV and Mtb infection respectively through a longitudinal analysis of samples taken pre and 1-year post treatment. ART increased the CD4 T-cell count in all IGRA$^+$ subjects tested (Supplementary Clinical File **1**). In addition, the absolute numbers of total LT Ag- and EC-specific IL-2, IL-10, IL-17F and MIP-1β but not IFN-γ and TNF-α CD4$^+$ T-cells was significantly enhanced by ART

(**Figure 4A**). ATT treatment of HIV-uninfected subjects with TB also highlighted significant enhancement of IL-10$^+$ LT Ag- and EC-specific and MIP-1β$^+$ LT Ag-specific CD4$^+$ T-cells; all other effectors were however not altered (**Figure 4B**). Therefore, ART treatment of HIV$^+$IGRA$^+$ subjects enhanced a broad range of total Mtb-specific T-cell effectors, whilst ATT treatment led to partial restoration of cytokine responses in HIV-uninfected subjects with TB. To note: ATT treatment of IGRA$^+$ subjects could not be conducted as ATT is only given to subjects with full blown TB in India.

ART and ATT restore regulatory Th17 responses in HIV$^+$ and TB patients

We next examined whether ART can specifically restore the skewed Mtb-specific Th17 response induced by HIV infection, and if ATT can restore these responses in TB treated patients. We observed that ART significantly reduced the absolute numbers of proinflammatory IFN-γ$^+$Th17 subsets and conversely increased regulatory IL-10$^+$Th17 subsets in response to both EC and LT Ag stimulation (**Figure 5A**). ATT also significantly enhanced absolute numbers of LT-Ag specific IL-10$^+$IL-17A$^+$, IL-10$^+$IL-17F$^+$ and IL-10$^+$IL-22$^+$ and EC-specific IL-10$^+$ IL-17F$^+$ Th17 subsets and conversely, a trend was noted for ATT treatment to suppress EC-specific IL-17F and IL-22 but not IL-17A cells that co-expressed IFN-γ (**Figure 5B**). In conclusion, both ART and ATT have the potential to restore the Mtb-specific regulatory Th17 response with ART also effective in dampening the Mtb-specific pro-inflammatory Th17 response in HIV-infected IGRA$^+$ subjects.

Loss of Mtb-specific effector cells in HIV-infected IGRA$^+$ subjects is not due to selective HIV infection associated with reduced expression of the anti-HIV chemokine, MIP-1β.

We next assessed if the selective early loss of Mtb-specific effectors in HIV$^+$IGRA$^+$ subjects, as shown in Figure 1, was due to higher HIV infection levels and associated absence of anti-HIV chemokine, MIP-1β expression by probing the viral load of antigen-specific CD4$^+$ T-cells that expressed high (CMV-specific) versus low levels (Mtb-specific) of MIP-1β. The CD4 count and viral loads of the subjects used for this analysis are shown in **Figure S9.** To note: all HIV$^+$ subjects with chronic HIV infection recruited to this study went on to subsequent ART treatment due to a declining CD4 T-cell count. An overview protocol used to capture antigen specific cells for analysis of viral load and cytokines is shown in Figure 6A. We used antigen

induced expression of CD154 and CD69 to capture specific cells as reported previously (**Bacher, et al., 2013**). Both $CD154^{+}CD69^{+}$ (antigen-specific activated) and $CD154^{-}CD69^{-}$ (un-activated control) memory ($CD45RA^{-}$) CD4 T-cells were captured by flow cytometry-based cell sorting after stimulation of PBMCs with Mtb antigens (EC or LT Ag) or with HIV-PTE (Env and Gag) or with CMVpp65 peptides. To verify the capture and stimulation efficacy, we first confirmed by qRT-PCR that the antigen activated subsets in each case expressed higher levels of IL-2 and IFN-γ, key cytokines induced by T-cell activation. For each antigen stimulation, we demonstrate that the $CD154^{+}CD69^{+}$ subset expressed significantly higher IFN-γ and IL-2 mRNA than the $CD154^{-}CD69^{-}$ counterpart (**Figures 6B and 6C**). We also demonstrate that Mtb-specific $CD154^{+}CD69^{+}$ cells do not express higher MIP-1β than their $CD154^{-}CD69^{-}$ counterpart, whereas CMV-specific cells did (**Figure 6D**). This qRT-PCR data complements the data in Figure 1 and confirms the captured Mtb-specific cells to be MIP-$1\beta^{low}$ relative to the captured CMV-specific cells.

Figure 7 provides the viral load data on the captured antigen specific cells. To quantify HIV DNA copy number, a standard curve was first optimized to detect as low as 1 copy of CD3 (reference gene) and HIV-1 LTR (**Figure S10**); the qPCR assay was sensitive for 6 copies of CD3 gene and 3 copies of HIV-1 LTR gene with 100% confidence as determined by testing genomic DNA isolated from ACH2 cells. After cut-off to exclude non-specific signals from low HIV-1 DNA loads (cut-off HIV-1 LTR gene qRT-PCR Signal Ct=30) and correlation of cell counts, the HIV-1 DNA copy number did not significantly vary in $CD154^{+}CD69^{+}$ T-cells across different antigen specificities (**Figure 7A**). Antigen stimulation in the absence of ART for 16 hr is recognised to be a weak stimulus for new HIV DNA synthesis; consistent with this, we show no significant difference in HIV DNA load between the $CD154^{+}CD69^{+}$ and it's the $CD154^{-}CD69^{-}$ counterpart in Mtb and HIV-specific cells; however there was a weak induction of HIV DNA in CMV-stimulated cells (**Figure 7B)**.

Cell associated HIV RNA was simultaneously quantified in each population by calculating the Fold Change (FC) of GAG gene expression in the $CD154^{+}CD69^{+}$ and the $CD154^{-}CD69^{-}$ counterpart relative to a negative control cell culture not exposed to any antigen. There was no significant difference in HIV RNA levels between $CD154^{+}CD69^{+}$ cells of different antigen specificities (**Figure 7C**). In addition, the HIV RNA levels in $CD154^{+}CD69^{+}$ versus $CD154^{-}CD69^{-}$ cells did not differ significantly, indicating no new burst of HIV Gag DNA translation following antigen stimulation (**Figure 7D**). We can confirm that this lack of induction of cell associated HIV RNA and HIV DNA at 16 hr post antigen stimulation was not due to inefficient activation as all antigens induced IFN-γ and IL-2 significantly in the $CD154^{+}CD69^{+}$ compared to the $CD154^{-}CD69^{-}$ counterpart (**Figures 6B and 6C**). Further, consistent with previous data (**Geldmacher et al., 2010**), $CD4^{+}$

T-cells stimulated with HIV PTE pool exhibited a higher proportion (41%) of cell associated HIV RNA compared to Mtb- and CMV-specific cells or total memory cells. Therefore, we provide strong evidence that HIV does not exclusively infect MIP-1β^{low} Mtb-specific cells from IGRA^{+} subjects with chronic HIV infection since equivalent viral burden were detected in MIP-1β^{hi} CMV-specific T-cells from the same subjects. In summary, MIP-1β levels do not seem to govern *in vivo* HIV infection levels of antigen-specific CD4^{+} T-cell subsets in IGRA^{+} subjects with chronic HIV infection.

DISCUSSION

This study provides fresh insights into the impact of HIV infection on the nature of the Mtb-specific $CD4^+$ T-cell response, particularly the Th17 response and unravels probable mechanisms that underpin why HIV infection is known to predispose $IGRA^+$ subjects to active TB, a topic of recognised global health importance.The increased vulnerability of Mtb-specific $CD4^+$ T-cells to HIV infection due to low MIP-1β expression is an attractive hypothesis for explaining why HIV selectively reduces the frequencies of Mtb-specific MIP-$1\beta^{low}$ effectors whilst preserving MIP-$1\beta^{hi}$ CMV-specific $CD4^+$ T-cell effectors **(see Geldmacher et al, 2010**). In keeping with previous data (**Amelio et al., 2019; Diedrich and Flynn, 2011; Murray et al., 2018)**, we confirm that HIV infection of $IGRA^+$ subjects selectively impairs Mtb-specific $CD4^+$ T-cell effectors expressing several key cytokines, including IFN-γ, IL-2, TNF-α, MIP-1β, IL-17 and IL-10 whilst preserving recall responses to CMV. Additionally, in this study we report that MIP-$1\beta^{low}$ Mtb-specific cells isolated from HIV-infected $IGRA^+$ subjects harboured similar viral load compared to MIP-$1\beta^{hi}$ CMV-specific cells. A critical explanation for this lack of concurrence between our viral load data and those of Geldmacher et al, may be linked to significant differences in the clinical stage of HIV-infected subjects studied. Geldmacher et al measured viral load in Mtb-specific and CMV-specific cells isolated from $IGRA^+$ subjects in the acute phase of HIV infection, before persistent loss of peripheral CD4 T-cell counts had occurred whereas we studied $IGRA^+$ subjects with chronic HIV infection with significantly lower CD4 T-cell counts than uninfected controls (**see Table 1**). We contend that in the scenario of rising viral load and declining $CD4^+$ counts as in the case of patients we studied, MIP-1β expression in CD4+ T-cells is less critical in setting a threshold for HIV infection and instead maybe driven by chronic T-cell activation.

HIV-mediated functional impairment of Mtb-specific $CD4^+$ T-cell immune responses may also contribute to erosion of anti-TB immunity and thereby predispose $IGRA^+$ subjects to TB (**Esmail et al., 2018**). Several studies have investigated the quality of Mtb-specific $CD4^+$ T-cell response in the context of HIV infection and reported a steady deterioration in the polyfunctionality of $CD4^+$ T-cells (**Day et al., 2017; Murray et al., 2018**). Likewise, we too observed significant impairment of the overall polyfunctional $CD4^+$ T-cell response especially to LT Ag in HIV^+IGRA^+ subjects, which was restored following ART. Beyond polyfunctionality, there is particular interest in understanding how HIV infection impacts Mtb-specific Th17 responses given their increasing importance in anti-TB immunity (**Rakshit et al., 2017, Rakshit et al., 2019; Dijkman et al., 2019**). In this study, we have addressed this issue and provide the first evidence that HIV infection

377 significantly reduces the frequency of Mtb-specific IL-10 and IL-17 co-expressing $CD4^+$ T-cells in $IGRA^+$
378 subjects. Understanding how HIV infection induces loss of $IL\text{-}17^+IL\text{-}10^+$ is important. One mechanism may
379 be linked to the efficient replication of HIV in Th17 cells in the gut (**Bixler and Mattapallil, 2013**). Gut-
380 homing $CXCR3^+CCR6^+CD4^+$ Th1/Th17 cells with increased TNF-α/IL-10 ratio are reportedly highly
381 permissive to HIV infection (**Gosselin et al., 2010; Alvarez et al., 2013**). Moreover, HIV is thought to
382 preferentially replicate in naïve precursors of regulatory Th17 cells that could possibly lead to distorted
383 polarization of Th17 cells towards the pathogenic phenotype in the presence of inflammatory environment
384 in the gut (**DaFonseca et al., 2015**). We therefore propose that by reducing the frequencies of anti-
385 inflammatory $IL\text{-}10^+$Th17 cells whilst sparing pathogenic $IFN\text{-}\gamma^+$Th17 cells, HIV creates a niche for
386 persistent replication. Further, the nature of HIV infection clearly influences the changes induced in the
387 Th17 response. Thus, LTNP subjects with a stable CD4 count in contrast to HIV^+IGRA^+ progressors, had
388 a robust Mtb-specific Th17 response that included largely anti-inflammatory $IL\text{-}10^+IL\text{-}17^+$ cells and few pro-
389 inflammatory $IFN\text{-}\gamma^+IL\text{-}17^+$ cells. ART treatment of chronic HIV-infected $IGRA^+$ progressors restored their
390 Mtb-specific responses, including polyfunctional cells and $IL\text{-}10^+IL\text{-}17^+$ anti-inflammatory cells, thus
391 confirming HIV infection to be a major driver of these immune changes.
392 Additional key mechanisms by which HIV may alter the balance of $IL\text{-}10^+$ and $IFN\text{-}\gamma^+$ Th17 subsets maybe
393 linked to HIV-driven changes in cytokines that are known to drive Th17 cell differentiation. A combination
394 of several factors involving lineage-specific polarizing cytokines like IL-23, IL-1β as well as IL-2, CCR6,
395 signaling mediators, transcription factors, metabolism, glucocorticoids, etc., are known to act in synergy to
396 regulate the Th17/Treg balance and inter-Th17 subset balance (**Yang et al., 2016; Seki and Nishizaw,**
397 **2016**). Interestingly in the context of TB, Th17 cells polarized under a hypoxic environment secrete IL-10 in
398 the TB granuloma (**Volchenkov et al., 2017**). Moreover, the paucity of the phenotypically naive $CD4^+$ T-
399 cell subsets, nTregs and $CD25^+CD127^+FoxP3^-$ enriched in Th17-lineage committed cells has been
400 associated with greater permissiveness to abortive and/or integrative HIV infection and maybe a potential
401 mechanism contributing to Th17 deficiency in HIV-infected subjects (**Gosselin et al., 2010**). Taken
402 together, limited expression of Th17-specific growth factors (e.g., IL-21, TGF-β) required for differentiation
403 and maintenance of regulatory Th17 cells in the inflammatory scenario of the HIV-infected gut may
404 contribute to the loss of Mtb-specific $IL\text{-}17^+IL\text{-}10^+$ cells in $IGRA^+$ subjects with chronic HIV infection.
405 To summarize, we provide first evidence that HIV infection disrupts the Mtb-specific Th17 response by
406 dramatically reducing the frequency of $IL\text{-}17^+$ cells that co-express IL-10, a loss that is pathogen driven and

407 can be restored by ART. In addition, our data indicates that HIV skews the Mtb-specific Th17 response
408 towards a pro-inflammatory profile in chronic IGRA$^+$ progressors, a pathogenic signature that is
409 characteristic of subjects with active TB, whereas the Mtb-specific regulatory Th17 response is retained in
410 HIV-infected IGRA$^+$ LTNP. Further analysis of HIV infection in Th17 subsets is warranted. Interestingly, our
411 results corroborate recent findings that show antibody-induced CD4$^+$ T-cell depletion alone is insufficient to
412 trigger the onset of TB in macaques with latent TB in the absence of HIV infection (**Bucsan et al., 2019**).
413 Further, chronically SIV-infected macaques with latent Mtb infection that eventually progressed to TB
414 displayed enhanced immune activation, inflammation and distorted CD4$^+$ T-cell differentiation phenotypes
415 compared to macaques that did not progress to TB even though both groups had undergone massive SIV-
416 induced CD4$^+$ T-cell depletion (**Bucsan et al., 2019**). Therefore, HIV-induced preferential loss of Mtb-
417 specific IL-10$^+$ regulatory CD4$^+$ Th17 cells may be detrimental to the host because a balanced immune
418 response is likely crucial for *Mtb* containment.
419

Acknowledgments

The authors thank the volunteers for participating in this study and acknowledge the contributions of clinical research workers at National Aids Research Institute and St John's Research Institute. We also thank the central IISc Biosafety Level 3 facility for help with flow cytometry. This work was funded principally by a Centre of Excellence grant to AV from the Department of Biotechnology, Govt. of India (No BT/PR10394/MED/29/1128/2016). We acknowledge additional funding for antigen synthesis by EC HORIZON2020, TBVAC2020 and EC FP7 EURIPRED (FP7-INFRA-2012 Grant Agreement No. 312661) to AV and THMO.

Author contributions

SR, NH, SVA and AV designed the study. SR performed the immunology experiments and analyzed flow cytometry data. NH and SVA performed the DNA and RNA PCR experiments and analyzed the data. VA helped with sorting, acquisition and data analysis. BKS and PNS helped with processing of blood from clinical cohorts. GF performed the main bioinformatic and immuno-informatic analyses. GDS, RP, MG and MT were clinical investigators. AJUK, CD and RGV collected clinical samples, provided the patient details and wrote the clinical methodology for the manuscript. THMO supplied the latency antigen recombinant proteins. SR, NH and SVA wrote the manuscript. SDeR, THMO, MT and AV edited the manuscript.

STAR METHODS

KEY RESOURCES TABLE

REAGENT or RESOURCE	SOURCE	IDENTIFIER
Antibodies		
V450 Mouse Anti-Human IFN-γ	BD Biosciences	Cat# 560371 Clone: B27
FITC Mouse Anti-Human TNF	BD Biosciences	Cat# 552889 Clone: MAb11
Alexa Fluor 700 anti-human IL-2	BioLegend	Cat# 500320 Clone: MQ1-17H12
Brilliant Violet 605 anti-human IL-17A	BioLegend	Cat# 512326 Clone: BL168
Brilliant Violet 650 Mouse Anti-Human IL-17F	BD Biosciences	Cat# 564264 Clone: O33-782
PE-Cy7 Mouse Anti-human IL-22	eBioscience	Cat# 25-7229-42 Clone: 22URTI
Brilliant Violet 786 Rat Anti-Human and ViralIL-10	BD Biosciences	Cat# 564049 Clone: JES3-9D7
PE Mouse Anti-Human MIP-1β	BD Biosciences	Cat# 550078 Clone: D21-1351
APC-H7 Mouse Anti-Human CD45RA	BD Biosciences	Cat# 560674 Clone: HI100
Alexa Fluor 647 anti-human CCR7	BioLegend	Cat# 353218 Clone: G043H7
Brilliant Violet 570 anti-human CD3	BioLegend	Cat# 300436 Clone: UCHT1
BUV395 Mouse Anti-Human CD4	BD Biosciences	Cat# 563550 Clone: SK3
Brilliant Violet 711 Mouse Anti-Human CD8	BD Biosciences	Cat# 563677 Clone: RPA-T8
Alexa Fluor 488 anti-human CD45RA	BioLegend	Cat# 304114 Clone: HI100
PE-Cy7 anti-human CCR7	BioLegend	Cat# 353226 Clone: G043H7
Brilliant Violet 510 anti-human CD14	BioLegend	Cat# 301842 Clone: M5E2
Brilliant Violet 510 anti-human CD19	BioLegend	Cat# 302242 Clone: HIB19
PE Mouse Anti-Human CD154	BD Biosciences	Cat# 555700 Clone: TRAP1
APC Mouse Anti-Human CD69	BD Biosciences	Cat# 340560 Clone: L78
CD40 antibody, Mouse Anti-human	Miltenyi Biotec	Cat# 130-094-133 Clone: HB14
Biological Samples		

PBMC samples from HIV-IGRA-, HIV-IGRA+, HIV+IGRA-, HIV+IGRA+ subjects, Pulmonary and extrapulmonary TB before and after ATT	St. John's Medical College Hospital, Bangalore, India	N/A
PBMC samples from HIV+IGRA+, HIV+IGRA+LTNP individuals	National AIDS Research Institute, Pune, India	N/A
Chemicals, Peptides, and Recombinant Proteins		
Histopaque 1077	Sigma Aldrich	Cat# 10771
Live/Dead Fixable Aqua Dead Cell Stain Kit	Invitrogen	Cat# L34966
ULtraComp eBeads	Invitrogen	Cat# 01-2222-42
Remel Phytohemagglutinin Purified	ThermoFisher Scientific	Cat# R30852801
SuperScript III Reverse Transcriptase	ThermoFisher Scientific	Cat# 18080093
ESAT6/CFP10 fusion protein	Department of Infectious Diseases, Leiden University Medical Center	N/A
Latency antigens (Rv1733c, RV1737c, Rv2029, RV2628)	Department of Infectious Diseases, Leiden University Medical Center	N/A
BD FastImmune CD28/CD49d Purified	BD Biosciences	Cat# 347690, Clone: L293/L25
Brefeldin A Solution (1,000X)	BioLegend	Cat# 420601
Monensin Solution (1,000X)	BioLegend	Cat# 420701
BD FACS Lysing Solution 10X Concentrate	BD Biosciences	Cat# 349202
BD Phosflow™ Perm/Wash Buffer I	BD Biosciences	Cat# 557885
Paraformaldehyde	Electron Microscopy Sciences	Cat# 15712-S
PepMix™ HCMVA (pp65)	JPT Peptide Technologies	Cat# PM-PP65-2
HIV-1 PTE Gag Peptide Pool 1	NIH AIDS Reagent Program	Cat# 12437
HIV-1 PTE-G Env Peptide Pool 1	NIH AIDS Reagent Program	Cat# 12698

Critical Commercial Assays		
TruCOUNT kit	BD Biosciences	Cat# 662415
Abbott RealTime HIV-1 Viral Load Assay	Abbott Molecular Inc.	Cat# 06L18-070
GAPDH Taq Man Gene Expression Assay (Hs99999905_m1)	ThermoFisher Scientific	Cat# 4351370
Taqman gene expression assay IFN-γ (Hs00989291_m1)	ThermoFisher Scientific	Cat# 4331182
Taqman gene expression assay IL-2 (Hs00174114_m1)	ThermoFisher Scientific	Cat# 4331182
Taqman gene expression assay MIP-1β (Hs99999148_m1)	ThermoFisher Scientific	Cat# 4331182
HIV GAG Custom TaqMan Probe Assay ID: AIHSQJI	ThermoFisher Scientific	Cat# 4331348
HIV-1 LTR Vanderg Custom TaqMan® Gene Expression Assay ID: APRWEWY	ThermoFisher Scientific	Cat# 4332078
HUM-CD3-Vanderg Custom TaqMan® Gene Expression Assay ID: APDJXRR	ThermoFisher Scientific	Cat# 4332078
Single Cell-to-CT™ qRT-PCR Kit	ThermoFisher Scientific	Cat# 4458236 & 4458237
Arcturus® PicoPure® DNA Extraction Kit	ThermoFisher Scientific	Cat# KIT0103
TaqMan Gene expression Master Mix	Applied Biosystems	Cat# 4369016
Amplitaq Gold 360 DNA Polymerase	Applied Biosystems	Cat# 4398823
Experimental Models: Cell Lines		
ACH-2 cells	Gift from Dr. Udaykumar Ranga, JNCASR, Bangalore.	Sreenath et al., 2010
HIV (pNL4-3 virus) infected Jurkat T-cells	Gift from Dr. Udaykumar Ranga, JNCASR, Bangalore.	Sreenath et al., 2010
Software and Algorithms		
GraphPad Prism 8.0.2	GraphPad Software	https://www.graphpad.com/

FlowJo version 9.9.6	Becton, Dickinson & Company	https://www.flowjo.com/
FACS DIVA	BD Bioscience	http://www.bdbiosciences.com/
COMPASS	Lin L et al. Nat Biotechnol. 2015; 33(6):610–616	www.bioconductor.org › bioc › COMPASS › inst › doc
Pestle v1.8	Roederer M et al. Cytometry A. 2011;79(2):167–174.	https://niaid.github.io/spice/
SPICE v5.1	Roederer M et al. Cytometry A. 2011;79(2):167–174.	https://niaid.github.io/spice/
7000 System SDS Software v1.2.3	Applied Biosystems	https://resource.thermofisher.com/pages 2013/WE111944/

RESOURCE AVAILABILITY

Lead Contact and Materials Availability

Further information and requests for resources and reagents should be directed to and will be fulfilled by the Lead Contact, Annapurna Vyakarnam (anna.vyakarnam@kcl.ac.uk). This study did not generate new unique reagents.

EXPERIMENTAL MODEL AND SUBJECT DETAILS

Study population

This study was performed in accordance with the relevant guidelines and regulations stated in the 'Declaration of Helsinki' and approved by the ethical review Committee of St. John's Medical College Hospital, Bangalore, India (Ref no: 55/2015) and the institutional ethics review board of National AIDS Research Institute (NARI/EC Protocol No.: 2012–06). A total of 205 individuals were recruited at St. John's Medical College Hospital, Bangalore, India and 78 at National AIDS Research Institute, Bhosari, Pune, Maharashtra, India between April 2015 and June 2017. After proper counselling, all participants provided written informed consent before enrolment. Relevant clinical information was documented in a proforma and 40 ml blood was drawn from each enrolled individual by venepuncture in ACD, EDTA or heparin tubes depending on the immune assays. The demographic, immunological, and virological

characteristics of the eight clinical groups are listed in Table 1. Detailed information of each participant has been included in Supplemental File 1.

HIV uninfected healthy IGRA$^+$ and IGRA$^-$ subjects

Healthcare workers of St. John's National Academy of Health Sciences were recruited through internal calls highlighting the nature and importance of the study. A commonly used interferon γ (IFN-γ) release assay (IGRA) for detecting *Mycobacterium tuberculosis* (Mtb) infection is the QuantiFERON-TB Gold In-tube test (QFT, Qiagen, Germany) (**Auguste et al., 2017**). It involves culturing blood cells with Mtb-specific antigens ESAT6, CFP10 and TB7.7 that do not cross react with antigens present in BCG vaccine or other non-tuberculous mycobacteria. A positive result is considered predictive of infection with Mtb. The kit also includes a positive control for T-cell activation and IFN-γ release (PHA) and a negative control (no antigen control) to adjust for spontaneous IFN-γ release. Study participants were screened based on this IGRA test and were stratified as IGRA$^+$ if their IFN-γ levels were greater than 0.35 IU/ml and IGRA$^-$ if the levels were below this cut-off. The detailed IGRA results have been summarized in the Supplemental Clinical File. All IGRA$^+$ subjects were asymptomatic for TB and had not received preventive/curative therapy for TB in the past. A total of 88 subjects were recruited and screened by the IGRA test, of which 26 were IGRA$^+$. Out of 26, 10 IGRA$^+$ subjects were included for the study; of which 80% were males with a median age of 30 years (25-38). Of the remaining 66, 10 IGRA$^-$ subjects served as uninfected healthy controls, of which 40% were males with a median age of 28 years (20-39). Healthcare workers in India do not undergo routine IGRA screening at the time of employment. Hence, ascertaining the duration for which our study subjects were IGRA$^+$ was not possible.

Pulmonary and Extrapulmonary TB

Subjects for this prospective study were enrolled at the Revised National Tuberculosis Program (RNTCP) clinic of St. John's Medical College and Hospital. According to the RNTCP guidelines, smear positivity is considered to be sufficient for diagnosis of pulmonary TB, chest radiograph and sputum culture is not necessary for TB diagnosis in India. Hence, diagnosis of pulmonary TB was ascertained by sputum smear microscopy and culture. Standard smear grading of 1$^+$, 2$^+$ and 3$^+$ was used to ascertain the bacterial burden. Smear negative cases of pulmonary TB cases were diagnosed and classified by

the treating clinician from plain chest radiographs as per the RNTCP standards. GeneXpert MTB/RIF assay (Cephid, USA), a nucleic-acid amplification (NAA) test of tissue sample approved by RNTCP, was used for confirmation of diagnosis. All patients included in the study were smear positive and positive for TB by GeneXpert. Rifampicin resistance by GeneXpert was an exclusion criterion. Sputum samples were collected for reconfirmation of TB diagnosis by GeneXpert MTB/RIF assay. Consenting adult patients meeting the above inclusion and exclusion criteria were included. A total of 5 cases of pulmonary TB were included in the study of which 80% were males with a median age of 34 years (30-66). A diagnosis of extrapulmonary TB was established from tissue specimens by Ziehl-Neelsen (ZN) staining for detection of AFB in tissue samples (obtained as surgical specimens/biopsies/FNACs). The site of extrapulmonary TB varied: 13 cases had cervical lymphadenitis and 2 had tubercular pleural effusions while the remaining four cases included one each of peritoneal TB, endometrial TB, intestinal TB and cold abscess. A total of 3 cases of extrapulmonary TB were included in the study of which 66.7% were males with a median age of 25 years (17-45). Study subjects were treatment naive at the time of enrolment and were counselled and initiated on standard anti-TB treatment (ATT) based on the directly observed treatment, short course (DOTS) regimen. Samples from 8 longitudinal donors (PTB, N=5 and EPTB, N=3) having undergone ATT for a period of 6 to 9 months were used in the study (**Table 1**). At a follow up visit 6-9 months from the start of ATT, blood was collected in EDTA or ACD tubes for isolation of PBMC.

HIV$^+$progressors, LTNP and HIV-TB coinfected patients

Subjects for this prospective study were enrolled at the ICMR-National AIDS Research Institute, Pune. HIV sero-positivity was confirmed by the standard HIV I and II ELISA test and western blot. CD4$^+$ T-cell counts were estimated by flow cytometry (FACSCalibur, Becton Dickinson, USA) as a part of routine investigations using TruCOUNT kit (Becton Dickinson, USA) at baseline and following therapy. HIV-1 RNA viral loads (copy number/ml) were evaluated in the stored plasma samples using the Abbott Real Time HIV-1 viral load assay (Abbott Molecular Inc., Des Plaines, IL, USA) on the m2000 System (Roche diagnostics, Germany) at all study visits according to the manufacturer's instructions. HIV positive subjects attending the antiretroviral clinic, voluntary counseling and testing center of St John's Hospital and Medical College, Bangalore and National AIDS Research Institute, Pune were recruited prospectively into this study. Only subjects with no prior history of treatment on anti-retroviral drugs (ART naïve) or post

exposure prophylaxis were included. Patients having a CD4 count below 350 cells/mm^3 were initiated on anti-retroviral treatment. A thorough physical examination was carried out to rule out opportunistic infections and concomitant tuberculosis. Whole blood was collected in EDTA vacutainer tubes from each patient before ART administration for measuring HIV-1 viral load and drug resistance genotyping. Patients were followed up every 6 months with repeat blood draws for samples from treatment naïve, confirmed HIV$^+$ subjects, negative for opportunistic infection and TB have been archived for this study with varying CD4 counts and virus loads. Progressors were defined as antiretroviral treatment (ART)-naïve HIV-infected patients with a CD4 count below 400 cells/mm^3 and were also simultaneously tested for TB specific secretary IFN-γ release by IGRA (Interferon Gamma Release Assay). A total of 10 HIV$^+$IGRA$^+$ subjects were enrolled in the study of which 50% were males with a median age of 37.5 years (27-56). A total of 10 HIV$^+$IGRA$^-$ subjects were enrolled in the study of which 70% were males with a median age of 31 years (24-47). Long term non progressors (LTNP) were defined as individuals with asymptomatic HIV infection for 7 or more years who stably maintained their CD4 count above 500 cells/mm^3 in absence of ART (**Kulkarni et al., 2017**). The mean seropositivity in LTNP cohort was 10.8 years with a range from 7 to 19 years. The CD4 counts of LTNPs at the study visit (median 823 cells/µl [IQR 679–1259]) were significantly higher than HIV+ progressors (median 352 cells/µl [IQR 289–540]). As expected, the plasma viral load values at the study visits were significantly lower in LTNPs (median 9943 HIV RNA copies/ml [IQR 0–19897]) when compared to the values from progressors (median 27926 [IQR 3510–516564]) (**Table 1**). LTNP subjects selected were also confirmed to be IGRA$^+$. A total of 7 LTNP subjects were enrolled in the study of which 42.8% were males with a median age of 36.5 years (33-48). The above cohorts were maintained at National AIDS Research Institute. HIV-TB coinfected patients were recruited at the RNTCP clinic of St. John's Medical College and Hospital, of which 8 were used for the study and 87.5% were males with a median age of 37 years (23-67).

Sample collection and processing

Peripheral blood mononuclear cells (PBMC) isolated from blood samples within 3 hr of blood draw by Histopaque (Sigma) density gradient centrifugation were cryopreserved in freezing medium containing 90% fetal calf serum (FCS) and 10% dimethyl sulfoxide (DMSO) and stored in liquid nitrogen until further usage.

Method Details

Intracellular cytokine staining (ICS) assay and multiparameter flow cytometry

ICS assay with antigen-stimulated PBMCs was performed as previously described (**Rakshit et al., 2017**). Briefly, cryopreserved PBMCs were thawed and seeded in 96-well round-bottom plates (Costar) at a concentration of 1×10^6 cells/well after 2hr of rest. Next, 1 µg/ml FastImmune CD28/CD49d (BD Biosciences) was added that enhances the cytokine production in $CD4^+$ T-cells in response to protein antigens and peptides by amplifying the signal for T-cell recognition (**Kagina et al., 2015**). Cells were either left unstimulated or stimulated overnight with antigens; 10 µg/ml of a pool of 4 DosR regulon-encoded LT Ag (Rv1733c, Rv1737c, Rv2029 and Rv2628) or secretory Mtb antigen ESAT6/CFP10 (EC) produced by Kees LMC Franken as recombinant proteins at the Department of Infectious Diseases, Leiden University Medical Center (**Franken et al., 2000**),1.7 µg/ml CMVpp65 peptide pool (JPT Peptide Technologies) and 1 µg/ml Phytohemagglutinin (PHA, Remel), followed by addition of brefeldin A and monensin (1X, BioLegend) for the last 16 hr. Next day, PBMCs were first stained with Live/Dead fixable Aqua dead cell stain or AviD (Invitrogen) to exclude dead cells from analysis, for 10 min at room temperature (RT). Details for all specific and titrated fluorochrome conjugated monoclonal antibodies to cell surface and intracellular markers used in the intracellular cytokine staining (ICS) assay are listed in the resource table. For analysis of T-cell responses, cells were stained with cell surface antibodies to CD45RA-APC-H7 (HI100) and CCR7-Alexa Fluor 647 (G043H7). Cells were then fixed with 1X FACS lysis buffer (BD Biosciences) for 10 min and permeabilized with 1X BD Perm/Wash buffer (BD Biosciences) for 20 min. For staining of intracellular cytokines, cells were incubated with a cocktail containing antibodies to CD3-BV570 (UCHT1), CD4-BUV395 (SK3), CD8-BV711 (RPA-T8), IFN-γ-V450 (B27), TNF-α-FITC (MAb11), IL-2-Alexa Fluor 700 (MQ1-17H12), IL-17A-BV605 (BL168), IL-17F-BV650 (O33-782), IL-10-BV786 (JES3-9D7), IL-22-PE-Cy7 (22URTI) and MIP-1β-PE (D21-1351). Antibody incubations were all performed at RT for 30 min in the dark. Cells were washed, fixed in 1% paraformaldehyde and kept at 4°C until acquisition.

Flow cytometry and data analysis

Samples were analyzed by flow cytometry using on BD FACSAria™ Fusion flow cytometer (BD Biosciences, San Jose, CA) and the associated BD FACSDiva™ version 8.0.1 software Cytometer Setting and Tracking (CST) beads (BD Biosciences) were acquired before each experiment to ensure that cytometer parameters remained consistent across all experiments. Stained samples were acquired with a standard stopping gate set at 200,000 CD3 lymphocytes. Negative and single-stained compensation beads (eBioscience) were acquired for each experiment, before sample acquisition, and used to calculate the compensation matrix. Data was then analyzed using the FlowJo version 9.9.6 software (FlowJo), Pestle v1.8, SPICE v5.1 (**Roederer et al., 2011**) as described previously. Briefly, $CD4^+$ T-cells expressing all possible combinations (256 subsets) of 8 effector cytokines were analyzed by Boolean gating in FlowJo. After careful analysis, the data was further analyzed by SPICE which identified 6 unique Th17 subsets that either expressed IFN-γ or IL-10 in combination with IL-17A/IL-17F/IL-22. These subsets were positive only for these cytokines and with no expression of other cytokines (IL-2, TNF-α and MIP-1β).

COMPASS analysis of flow cytometry data

Cell counts were analyzed using the COMPASS algorithm as described. Briefly, COMPASS is a statistical model developed for high-dimensional flow cytometry data analysis that can detect antigen-specific changes across all observable functional T-cell subsets, without the need to limit the analysis to very specific subsets based on expected biological significance (**Lin et al., 2015**). In COMPASS, responses are quantified using posterior probabilities that summarize for each subject and subset the evidence that the corresponding response is Ag specific by comparing the proportion of cytokine-positive cells in the Ag sample to the corresponding proportion in the control sample. Polyfunctionality scores were calculated from posterior responses probabilities, summarizing a subject's entire T-cell functionality profile into a single number. In this study, we have applied COMPASS to each of the antigens in $CD4^+$ T-cell subsets leading to 20 analyses. Each one of the analyses was unbiased and considered all of the 256 possible cytokine functions (defined as Boolean combination). In order to evaluate differences in polyfunctionality between groups, a linear model estimating the group wise mean polyfunctionality scores was fit to each antigen and the difference between $IGRA^+$ and other groups was tested (Wald test, null:, two-sided test). Resulting p-values were adjusted for multiple testing (across all 60 tests and models) to control the FDR (false discovery rate) using the method of Benjamini & Hochberg (**Green and Diggle, 2007**). Significant differences were

called at the 5% FDR level. Magnitudes of T-cell responses were calculated independent of COMPASS as the maximum of zero or the proportion of gated events in the stimulated condition minus the proportion of gated events in the unstimulated condition.

Capture of antigen-specific CD4$^+$ T-cells

Cryopreserved PBMCs were thawed, rested for 2 hr and plated in U bottom 96 well plate at 1 × 10^6/ well., Cells were then blocked with 0.5 µg/ml CD40 (HB14) antibody for 15 min at 37°C. Blocking antibody to CD40 prevents CD154 downregulation and thereby facilitates capture of CD154$^+$ antigen specific CD4$^+$ T-cells (**Frentsch et al., 2005**). Next, anti-CD28/CD49d costimulatory antibody and antigens (CMVpp65, EC, LT Ag and HIV-PTE (Env-1-3, and Gag 1-2) pools were added for 16 hr. Next day, PBMCs were stained with AviD the monoclonal antibodies to CD3-BV570 (UCHT1), CD4-BUV395 (SK3), CD8-BV711 (RPA-T8), CD45RA-Alexa Fluor 488 (HI100), CCR7-PE-Cy7 (G043H7), CD14-BV510 (M5E2), CD19-BV510 (HIB19), CD154-PE (TRAP1), CD69-APC (L78) listed in resource table and sorted on a BD FACSAria Fusion flow cytometer with a 100 µm nozzle, 15 psi, 100 rpm agitation at 4°C with a flow rate of 3000–6000 events/sec. Cells were sorted using FACS Diva software to isolate antigen-specific (CD3$^+$CD4$^+$CD154$^+$CD69$^+$) and resting (CD3$^+$CD4$^+$CD154$^-$CD69$^-$) CD4$^+$ T-cells, referred to as CD154$^+$CD69$^+$ and CD154$^-$CD69$^-$ henceforth, for quantification of cell-associated HIV DNA and HIV RNA .

DNA isolation

DNA isolation was performed using Arcturus Pico Pure DNA kit (ThermoFisher Scientific) as per manufacturer's instructions. Isolated DNA was directly used in the pre-amplification PCR performed in the same tube for both HIV-1 LTR and human CD3 gene.

Real Time quantitative PCR (qPCR) for quantification of total cell-associated HIV DNA

Total cell associated HIV DNA was quantified by the method described previously (**Vandergeeten et al., 2014**) with some modifications. qPCR was performed using custom synthesized HIV-1 LTR and human CD3 gene based TaqMan Gene expression assays and TaqMan Gene expression Master Mix (Applied Biosystems) on the StepOne Plus Real-Time PCR Detection System (Applied Biosystems) according to

629 the manufacturer's recommendations. Before qPCR, DNA prepared from sorted cells was subjected to pre-
630 amplification PCR performed in single tube of 50 μl PCR reaction volume for both HIV-1 LTR and human
631 CD3 gene using Amplitaq Gold 360 DNA Polymerase. The absolute quantity of cell associated HIV DNA
632 was calculated based on standard curves of ACH-2 cells, which carry a single copy of the integrated HIV
633 genome, which were used to generate standard curves for both HIV-1 LTR and human CD3 gene (**Figure**
634 **S10**). Series of ten-fold dilutions of ACH-2 cells DNA corresponding to 3×10^5 to 3 HIV-1 DNA copies per
635 reaction was included in each experiment in order to generate standard curves for both HIV-1 LTR as well
636 as human CD3 gene. Individual standard curves from each experiment were used to determine the copy
637 number of HIV-1 LTR and human CD3 gene respectively. All samples were analyzed in duplicate. The
638 result of the cell associated HIV-1 DNA quantification was expressed as number of HIV DNA copies per
639 million $CD4^+$ T-cells. Two negative controls are typically included in each plate: DNase/RNase-free water,
640 as a control for the PCR (no template control, NTC) and DNA extracted from the HIV uninfected Jurkat T-
641 cells. Additionally, DNA extracted from sorted $CD4^+$ T-cells from PBMCs of HIV sero-negative healthy
642 individuals were also included in few experiments to demonstrate the specificity of HIV-1 LTR qPCR assay.
643 DNA extracted from the HIV (pNL4-3 virus) infected Jurkat T-cells was also included as positive control in
644 each assay. Human CD3 gene was quantified in order to determine the input level of cellular DNA in the
645 sample and was used as an endogenous reference to normalize variations due to differences in the cell
646 count or DNA extraction. Total HIV DNA copies per million cells were determined by calculating the number
647 of cells from the human CD3 gene copy number which is present as 2 copies of CD3 gene per cell.
648
649 **Linearity, specificity and sensitivity of qPCR assay to quantify cell-associated HIV DNA**
650 The dynamic range of the assay for both HIV-1 LTR and Human CD3 gene encompassed at least 6 orders
651 of magnitude, with a strong linear relationship (r2 >0.998) between the Ct values and log10 input number
652 of gene copies. HIV-1 LTR signal was never detected in any of the experiments in the negative control DNA
653 (DNA of HIV negative Jurkat T-cells and sorted CD4 T-cells from PBMCs of HIV sero-negative healthy
654 person) indicating the specificity of the qPCR assay for HIV-1 LTR. For DNA from HIV negative Jurkat T-
655 cells the median Ct value for human CD3 gene from 10 experiments was 22.36 (Range: 19.95 – 23.52)
656 and no HIV-1 LTR signal was detected in any of the 10 experiments. When DNA of sorted CD4 T-cells from
657 PBMCs from HIV sero-negative healthy donor were tested in two experiments, the mean Ct for human CD3
658 was 21.41 (SD 0.26) and no HIV-1 LTR signal was detected in both the experiments. Both human CD3 and

HIV-1 LTR qPCR assays were highly sensitive and could detect as low as single copy of the target gene in the 20 μl of template DNA used in the pre-amplification PCR reaction.

Relative quantification of cytokines and cell-associated HIV-1 RNA

Single Cell-to-CT kit was used to quantify cell-associated HIV-1 RNA. For each stimulation 100 to 250 cells ($CD154^+CD69^+$ or $CD154^-CD69^-$) were directly sorted into 10μl single cell lysis solution containing 1μl of single cell DNase I. Single Cell Stop solution (1μl) was added to stop the lysis reaction, followed by a 2min incubation at RT prior to freezing at -20°C. cDNA synthesis and pre-amplification were done according to manufacturer's instructions. TaqMan Probes used for pre-amplification (and later used for qPCR) were: GAPDH (reference gene, Hs99999905_m1), GAG mRNA (in-house custom designed), IFN-γ (Hs00989291_m1), IL-2 (Hs00174114_m1) and MIP-1β (Hs99999148_m1). After pre-amplification, the samples were stored at -20°C. For gene expression analysis of the cDNA, a downscaled version of the qPCR protocol supplied with the Single Cell-to-CT kit was used, with reactions performed in 10μl, comprising of 5μl 2X TaqMan Gene Expression Master Mix supplied with the kit, 5 times diluted cDNA sample, 0.5μl of 20X TaqMan probes and nuclease-free water. All qPCR reactions were performed in a 96-well plate (Eppendorf), in duplicate and Cq values were averaged. Relative copy number (RCN_{gene}) was calculated against CT values of GAPDH mRNA levels in each sample (equation 1). All the gene expressions (GAG, IFN-γ, IL-2 and MIP-1β are represented as Fold Change (FC_{gene}, equation 2) by dividing RCN_{gene} by the median RCN of the same genes from unstimulated cells ($RCN_{med.unstimulated}$). Data is represented irrespective of the sorted $CD4^+$ cell type.

$$RCN_{gene} = power\ (2, -(\Delta CTgene - \Delta CTGAPDH)) \quad (1)$$

$$FC_{gene} = RCN_{gene} / RCN_{med.unstimulated} \quad (2)$$

Clinical subjects with GAPDH CT in the range of 15 to 27 were considered. In order to confirm that the CT values for GAG-gene were indeed equivalent to actual gene expression and not any non-specific signal, control experiments were carried out using uninfected PBMCs and 250 cells were sorted for unstimulated and antigen-stimulated cells. qPCR was carried out on these samples for the above mentioned TaqMan probes. The GAG gene RCN of uninfected PBMCs were considered to be non-specific binding (background noise) of TaqMan probe and clinical subjects with GAG gene CT to be greater than 32 were removed and GAG gene CT equivalent to undetermined were given a CT of 32 for further statistical analysis.

Statistical Analysis

All antigen-stimulated wells were adjusted for non-specific responses by background subtraction (media alone). Statistical analyses were performed and graphs were created using GraphPad Prism software version 6.0.7 (GraphPad, La Jolla, CA). Paired longitudinal comparisons within the same group were done using the Wilcoxon matched-pairs signed rank test. Comparisons across two treatment groups were done using unpaired Mann–Whitney test. The p values were reported unadjusted, but were interpreted after adjustment using the Bonferroni correction for multiple comparisons. Statistical analyses across seven clinical groups was performed using a one-way ANOVA nonparametric Kruskal–Wallis test and corrected by Dunn's test for multiple comparisons.

REFERENCES

Acosta-Rodriguez, E. V., Rivino, L., Geginat, J., Jarrossay, D., Gattorno, M., Lanzavecchia, A., Sallusto, F., and Napolitani, G. (2007). Surface phenotype and antigenic specificity of human interleukin 17-producing T helper memory cells. Nature Immunology. *8*, 639–646.

Ahmed, A., Rakshit, S., and Vyakarnam, A. (2016). HIV-TB co-infection: mechanisms that drive reactivation of Mycobacterium tuberculosis in HIV infection. Oral Dis. *22*, 53-60.

Alvarez, Y., Tuen, M., Shen, G., Nawaz, F., Arthos, J., Wolff, M.J., Poles, M.A., and Hioe, C.E. (2013). Preferential HIV infection of CCR6+ Th17 cells is associated with higher levels of virus receptor expression and lack of CCR5 ligands. J. Virol. *87*, 10843–10854.

Amelio, P., Portevin, D., Hella, J., Reither, K., Kamwela, L., Lweno, O., Tumbo, A., Geoffrey, L., Ohmiti, K., Ding, S., and Pantaleo, G. (2019). HIV Infection Functionally Impairs Mycobacterium tuberculosis-Specific CD4 and CD8 T-Cell Responses. J Virol. *93*, e01728-18.

Arroyo, L., Rojas, M., Franken, K. L., Ottenhoff, T. H., and Barrera, L. F. (2016). Multifunctional T Cell Response to DosR and Rpf Antigens Is Associated with Protection in Long-Term Mycobacterium tuberculosis-Infected Individuals in Colombia. Clin Vaccine Immunol. *23*, 813-824.

Auguste, P., Tsertsvadze, A., Pink, J., Court, R., McCarthy, N., Sutcliffe, P., and Clarke, A. (2017). Comparing interferon-gamma release assays with tuberculin skin test for identifying latent tuberculosis infection that progresses to active tuberculosis: systematic review and meta-analysis. BMC infectious diseases. *17*, 200.

Bacher, P., and Scheffold, A. (2013). Flow-cytometric analysis of rare antigen-specific T cells. Cytometry A. *83,* 692-701.

Bell, L. C., and Noursadeghi, M. (2018). Pathogenesis of HIV-1 and Mycobacterium tuberculosis co-infection. Nature Reviews Microbiology. *16*, 80-90.

Bixler, S. L., and Mattapallil, J. J. (2013). Loss and dysregulation of Th17 cells during HIV infection. Clin. Dev. Immunol. *2013*, 852418.

Bronke, C., Palmer, N.M., Jansen, C.A., Westerlaken, G.H., Polstra, A.M., Reiss, P., Bakker, M., Miedema, F., Tesselaar, K., and Baarle, D.V. (2005). Dynamics of cytomegalovirus (CMV)-specific T cells in HIV-1-infected individuals progressing to AIDS with CMV end-organ disease. J Infect Dis. *191*, 873-880.

729 Bucşan, A.N., Chatterjee, A., Singh, D.K., Foreman, T.W., Lee, T.H., Threeton, B., Kirkpatrick, M.G.,
730 Ahmed, M., Golden, N., Alvarez, X., et al. (2019). Mechanisms of reactivation of latent tuberculosis
731 infection due to SIV coinfection. J Clin Invest. *129*, 5254-5260.
732 Caetano, D. G., de Paula, H., Bello, G., Hoagland, B., Villela, L. M., Grinsztejn, B., Veloso, V. G.,
733 Morgado, M. G., Guimarães, M. L., and Côrtes, F. H. (2020). HIV-1 elite controllers present a high
734 frequency of activated regulatory T and Th17 cells. PloS one. *15*, e0228745.
735 Carpenter, C., Sidney, J., Kolla, R., Nayak, K., Tomiyama, H., Tomiyama, C., Padilla, O.A., Rozot, V.,
736 Ahamed, S.F., Ponte, C., et al. (2015). A side-by-side comparison of T cell reactivity to fifty-nine
737 Mycobacterium tuberculosis antigens in diverse populations from five continents. Tuberculosis (Edinb).
738 *95*, 713–721.
739 Chiacchio, T., Petruccioli, E., Vanini, V., Cuzzi, G., La Manna, M. P., Orlando, V., Pinnetti, C.,
740 Sampaolesi, A., Antinori, A., Caccamo, N., and Goletti, D. (2018). Impact of antiretroviral and
741 tuberculosis therapies on CD4+ and CD8+ HIV/M. tuberculosis-specific T-cell in co-infected subjects.
742 Immunology letters, *198*, 33–43.
743 Ciccone, E.J., Greenwald, J.H., Lee, P.I., Biancotto, A., Read, S.W., Yao, M.A., Hodge, J.N.,
744 Thompson, W.L., Kovacs, S.B., Chairez, C.L., and Migueles, S.A. (2011). CD4+ T cells, including Th17
745 and cycling subsets, are intact in the gut mucosa of HIV-1-infected long-Term nonprogressors. J Virol.
746 *85*, 5880–5888.
747 Coppola, M., and Ottenhoff, T.H. (2018). Genome wide approaches discover novel Mycobacterium
748 tuberculosis antigens as correlates of infection, disease, immunity and targets for vaccination. Semin
749 Immunol. *39*, 88-101.
750 DaFonseca, S., Niessl, J., Pouvreau, S., Wacleche, V. S., Gosselin, A., Cleret-Buhot, A., Bernard, N.,
751 Tremblay, C., Jenabian, M. A., Routy, J. P., and Ancuta, P. (2015). Impaired Th17 polarization of
752 phenotypically naive CD4(+) T-cells during chronic HIV-1 infection and potential restoration with early
753 ART. Retrovirology. *12*, 38.
754 Day, C. L., Abrahams, D. A., Harris, L. D., van Rooyen, M., Stone, L., de Kock, M., and Hanekom, W.
755 A. (2017). HIV-1 Infection Is Associated with Depletion and Functional Impairment of Mycobacterium
756 tuberculosis-Specific CD4+ T Cells in Individuals with Latent Tuberculosis Infection. J Immunol. *199*,
757 2069-2080.

Day, C. L., Mkhwanazi, N., Reddy, S., Mncube, Z., van der Stok, M., Klenerman, P., and Walker, B. D. (2008). Detection of polyfunctional Mycobacterium tuberculosis-specific T cells and association with viral load in HIV-1-infected persons. J Infect Dis. *197*, 990–999.

Diedrich, C.R., and Flynn, J.L. (2011). HIV-1/ Mycobacterium tuberculosis Coinfection Immunology: How does HIV-1 Exacerbate Tuberculosis? Infect Immun. *79*, 1407–1417.

Dijkman, K., Sombroek, C.C., Vervenne, R.A., Hofman, S.O., Boot, C., Remarque, E.J., Kocken, C.H., Ottenhoff, T.H., Kondova, I., Khayum, M.A., et al. (2019). Prevention of tuberculosis infection and disease by local BCG in repeatedly exposed rhesus macaques. Nat Med. *25*, 255–262.

Douek, D. C., Picker, L. J., and Koup, R. A. (2003). T cell dynamics in HIV-1 infection. Annu Rev Immunol. *21*, 265-304.

Elhed, A., and Unutmaz, D. (2010). Th17 cells and HIV infection. Current opinion in HIV and AIDS. *5*, 146–150.

Esmail, H., Riou, C., du Bruyn, E., Lai, R.P.J., Harley, Y.X., Meintjes, G., Wilkinson, K.A., and Wilkinson, R.J. (2018). The Immune Response to Mycobacterium tuberculosis in HIV-1-Coinfected Persons. Annu Rev Immunol. *36*, 603-638.

Franken, K.L., Hiemstra, H.S., van Meijgaarden, K.E., Subronto, Y., den Hartigh, J., Ottenhoff, T.H., and Drijfhout, J.W. (2000). Purification of his-tagged proteins by immobilized chelate affinity chromatography: the benefits from the use of organic solvent. Protein Expr Purif. *18*, 95-99.

Frentsch, M., Arbach, O., Kirchhoff, D., Moewes, B., Worm, M., Rothe, M., Scheffold, A., and Thiel, A. (2005). Direct access to CD4+ T cells specific for defined antigens according to CD154 expression. Nat Med. *11*, 1118–1124.

Foreman, T. W., Mehra, S., LoBato, D. N., Malek, A., Alvarez, X., Golden, N. A., Bucşan, A. N., Didier, P. J., Doyle-Meyers, L. A., Russell-Lodrigue, K. E., et al. (2016). CD4+ T-cell-independent mechanisms suppress reactivation of latent tuberculosis in a macaque model of HIV coinfection. PNAS *113*, E5636–E5644.

Geldmacher, C., and Koup, R.A. (2012). Pathogen-specific T cell depletion and reactivation of opportunistic pathogens in HIV infection. Trends Immunol. *33*, 207-214.

Geldmacher, C., Ngwenyama, N., Schuetz, A., Petrovas, C., Reither, K., Heeregrave, E.J., Casazza, J.P., Ambrozak, D.R., Louder, M., Ampofo, W., et al. (2010). Preferential infection and depletion of Mycobacterium tuberculosis-specific CD4+ T cells after HIV-1 infection. J Exp Med. *207*, 2869-2881.

788 Gideon, H. P., Phuah, J., Myers, A. J., Bryson, B. D., Rodgers, M. A., Coleman, M. T., Maiello, P.,
789 Rutledge, T., Marino, S., Fortune, S. M., et al. (2015). Variability in tuberculosis granuloma T cell
790 responses exists, but a balance of pro- and anti-inflammatory cytokines is associated with sterilization.
791 PLoS Pathog. *11*, e1004603.
792 Gosselin, A., Monteiro, P., Chomont, N., Diaz-Griffero, F., Said, E.A., Fonseca, S., Wacleche, V., El-
793 Far, M., Boulassel, M.R., Routy, J.P., et al. (2010). Peripheral Blood CCR4+CCR6+and
794 CXCR3+CCR6+ CD4+ T Cells Are Highly Permissive to HIV-1 Infection. J Immunol (Baltimore, Md:
795 1950). *184*, 1604-1616.
796 Green, G.H., and Diggle, P.J. (2007). On the operational characteristics of the Benjamini and Hochberg
797 False Discovery Rate procedure. Stat Appl Genet Mol Biol. 6: Article 27.
798 Kagina, B. M., Mansoor, N., Kpamegan, E. P., Penn-Nicholson, A., Nemes, E., Smit, E., Gelderbloem,
799 S., Soares, A. P., Abel, B., Keyser, A., et al (2015). Qualification of a whole blood intracellular cytokine
800 staining assay to measure mycobacteria-specific CD4 and CD8 T cell immunity by flow cytometry. J
801 Immunol Methods., *417*, 22–33.
802 Kalokhe, A. S., Adekambi, T., Ibegbu, C. C., Ray, S. M., Day, C. L., and Rengarajan, J. (2015). Impaired
803 degranulation and proliferative capacity of Mycobacterium tuberculosis-specific CD8+ T cells in HIV-
804 infected individuals with latent tuberculosis. J infect Dis, *211*, 635–640.
805 Kulkarni, A., Kurle, S., Shete, A., Ghate, M., Godbole, S., Madhavi, V., Kent, S.J., Paranjape, R., and
806 Thakar, M. (2017). Indian Long-term Non-Progressors Show Broad ADCC Responses with Preferential
807 Recognition of V3 Region of Envelope and a Region from Tat Protein. Front Immunol. *8*, 5.
808 Kuroda, M. J., Sugimoto, C., Cai, Y., Merino, K. M., Mehra, S., Araínga, M., Roy, C. J., Midkiff, C. C.,
809 Alvarez, X., Didier, E. S., and Kaushal, D. (2018). High Turnover of Tissue Macrophages Contributes
810 to Tuberculosis Reactivation in Simian Immunodeficiency Virus-Infected Rhesus Macaques. The
811 Journal of infectious diseases, *217*, 1865–1874.
812 Lawn, S. D., and Wilkinson, R. J. (2015). ART and prevention of HIV-associated tuberculosis. The
813 lancet. HIV, *2*, e221–e222.
814 Lin, L., Finak, G., Ushey, K., Seshadri, C., Hawn, T.R., Frahm, N., Scriba, T.J., Mahomed, H.,
815 Hanekom, W., Bart, P.A., et al. (2015). COMPASS identifies T-cell subsets correlated with clinical
816 outcomes. Nat Biotechnol. *33*, 610–616.

817 Lin, P. L., and Flynn, J. L. (2018). The End of the Binary Era: Revisiting the Spectrum of Tuberculosis. J
818 Immunol. *201*: 2541–2548.
819 Mercer, F., Khaitan, A., Kozhaya, L., Aberg, J. A., and Unutmaz, D. (2014). Differentiation of IL-17-
820 producing effector and regulatory human T cells from lineage-committed naive precursors. J Immunol.
821 *193*, 1047-1054.
822 Murray, L.W., Satti, I., Meyerowitz, J., Jones, M., Willberg, C.B., Ussher, J.E., Goedhals, D., Hurst, J.,
823 Phillips, R.E., McShane, H., et al. (2018). Human Immunodeficiency Virus Infection Impairs Th1 and
824 Th17 Mycobacterium tuberculosis -Specific T-Cell Responses. J Infect Dis. *217*, 1782-1792.
825 Okoye, A. A., and Picker, L. J. (2013). CD4(+) T-cell depletion in HIV infection: mechanisms of
826 immunological failure. Immunol Rev. *254*, 54-64.
827 Pawlowski, A., Jansson, M., Sköld, M., Rottenberg, M. E., and Källenius, G. (2012). Tuberculosis and
828 HIV co-infection. PLoS pathogens. *8*.
829 Rakshit, S., Adiga, V., Nayak, S., Sahoo, P.N., Sharma, P.K., van Meijgaarden, K.E., Uk, J., A.J., Dhar,
830 C., Souza, G.D., Finak, G., et al. (2017). Circulating Mycobacterium tuberculosis DosR LT Ag-specific,
831 polyfunctional, regulatory IL-10(+) Th17 CD4+ T-cells differentiate latent from active tuberculosis. Sci
832 Rep. *7*, 11948.
833 Rakshit, S., Ahmed, A., Adiga, V., Sundararaj, B.K., Sahoo, P.N., Kenneth, J., D'Souza, G., Bonam,
834 W., Johnson, C., Franken, K.L., et al. (2019). BCG revaccination boosts adaptive polyfunctional
835 Th1/Th17 and innate effectors in IGRA+ and IGRA- Indian adults. JCI Insight. *4*, e130540.
836 Riou, C., Bunjun, R., Müller, T.L., Kiravu, A., Ginbot, Z., Oni, T., Goliath, R., Wilkinson, R.J., and
837 Burgers, W.A. (2016). Selective reduction of IFN--γ single positive mycobacteria-specific CD4+ T cells
838 in HIV-1 infected individuals with latent tuberculosis infection. Tuberculosis (Edinb.) *101*, 25–30.
839 Roederer, M., Nozzi, J.L., and Nason, M.C. (2011). SPICE: exploration and analysis of post-cytometric
840 complex multivariate datasets. Cytometry A. *79*, 167–174.
841 Seki, R., and Nishizawa, K. (2016). Factors regulating Th17 cells: a review. Biomed Res and Clin Pract.
842 *1*, 126-147.
843 Sreenath, K., Pavithra, L., Singh, S., Sinha, S., Dash, P. K., Siddappa, N. B., Ranga, U., Mitra, D., and
844 Chattopadhyay, S. (2010). Nuclear matrix protein SMAR1 represses HIV-1 LTR mediated transcription
845 through chromatin remodeling. Virology. *400*, 76–85.

Thakar, M.R., Abraham, P.R., Arora, S., Balakrishnan, P., Bandyopadhyay, B., Joshi, A.A., Devi, K.R., Vasanthapuram, R., Vajpayee, M., Desai, A., et al. (2011). Establishment of reference CD4+ T cell values for adult Indian population. AIDS Res Ther. *8*, 35.

Trinchieri G. (2001). Regulatory role of T cells producing both interferon gamma and interleukin 10 in persistent infection. J Exp Med. *194*, F53–F57.

Vandergeeten, C., Fromentin, R., Merlini, E., Lawani, M.B., DaFonseca, S., Bakeman, W., McNulty, A., Ramgopal, M., Michael, N., Kim, J.H., et al. (2014). Cross-clade ultrasensitive PCR-based assays to measure HIV persistence in large-cohort studies. J Virol. *88*, 12385-12396.

Volchenkov, R., Nygaard, V., Sener, Z., and Skålhegg, B.S. (2017). Th17 Polarization under Hypoxia Results in Increased IL-10 Production in a Pathogen-Independent Manner. Front Immunol. *8*, 698.

World Health Organization (WHO). HIV factsheets 2019. http://www.who.int/news-room/fact-sheets/detail/hiv-aids. Date last updated: 25 November 2019. Date last accessed: September 12, 2020.

World Health Organization Global Tuberculosis Report 2019, World Health Organization. https://www.who.int/tb/publications/global_report/en/.

Yang, B.H., Hagemann, S., Mamareli, P., Lauer, U., Hoffmann, U., Beckstette, M., Föhse, L., Prinz, I., Pezoldt, J., Suerbaum, S., et al. (2016). Foxp3(+) T cells expressing RORγt represent a stable regulatory T-cell effector lineage with enhanced suppressive capacity during intestinal inflammation. Mucosal Immunol. *9*, 444-457.

Yang, X., Jiao, Y.M., Wang, R., Ji, Y.X., Zhang, H.W., Zhang, Y.H., Chen, D.X., Zhang, T., and Wu, H. (2012). High CCR5 density on central memory CD4+ T cells in acute HIV-1 infection is mostly associated with rapid disease progression. PLoS One. *7*, e49526.

FIGURE LEGENDS

Figure 1: HIV infection impairs the expression of effector cytokines in Mtb-specific $CD4^+$ T-cells. PBMCs from (A) HIV^-IGRA^+ (N=10, green) vs. HIV^+IGRA^+ (N=10, red) and (B) HIV^-IGRA^- (N=10, brown) vs. HIV^+IGRA^- (N=10, blue) subjects were stimulated overnight with EC (10µg/ml), LT Ag (10µg/ml), CMVpp65 (1.7µg/ml) and PHA (1µg/ml). All HIV^+ subjects were initiated on ART after collection of blood at baseline post diagnosis. $CD3^+CD4^+$ T-cells were analyzed for intracellular expression of IFN-γ, IL-2, MIP-1β, TNF-α, IL-10 and IL-17F in a standard ICS assay. Frequencies of cytokine-producing total $CD4^+$ T-cells were obtained after background subtraction of values from unstimulated control. Absolute numbers of antigen-specific $CD4^+$ T-cells were calculated by multiplying the frequencies of cytokine-positive $CD4^+$ T-cells by the total CD4 T-cell count. Box-and-whisker plots show the inter-quartile range and horizontal bars represent the median absolute numbers of total cytokine-positive $CD4^+$ T-cells. Statistical analysis was performed by Mann-Whitney two-tailed t test: with Bonferroni's correction for multiple comparisons.

Figure 2: COMPASS and SPICE analysis reveals HIV infection reduces $CD4^+$ polyfunctional responses to EC and LT Ag in $IGRA^+$ and $IGRA^-$ subjects. PBMCs were stimulated overnight with EC and LT Ag and $CD3^+CD4^+$ T-cells were analyzed for intracellular expression of IFN-γ, IL-2, MIP-1β, TNF-α, IL-10 and IL-17F in a standard ICS assay. All HIV^+ subjects were initiated on ART after collection of blood at baseline post diagnosis. Boolean gates were created from the individual cytokine (listed above) in FlowJo to divide responding cells into 64 distinct subsets corresponding to all possible combinations of these functions and the data was analyzed using COMPASS and SPICE software. (A) Box plots show Mtb-specific CD4+ T-cell polyfunctionality scores (PFS) analyzed by COMPASS in HIV^-IGRA^+ (green), HIV^+IGRA^+ (red), and HIV^+IGRA^- (blue). For each antigen, pairwise differences between HIV^-IGRA^+ and other groups were based on a group wise linear model fit to the PFS (null: $\beta_{group}-\beta_{HIV\text{-}IGRA^+}=0$ two-sided test) and p-values adjusted for multiple testing (see methods). (B) SPICE analyses for in-depth phenotypic profiling of Mtb-specific $CD4^+$ T-cells in HIV^-IGRA^+ (N=10), HIV^+IGRA^- (N=10), and HIV^+IGRA^+ (N=10) subjects. Each slice of the pie corresponds to a distinct combination of 6 cytokines (IFN-γ, IL-2, TNF-α, IL-17F, IL-10 and MIP-1β) produced in response to EC and LT Ag stimulation. The pie charts depict the mean frequency for each of the 64 possible phenotypic profiles of Mtb-specific $CD4^+$ T-cells. The arcs surrounding the pie charts indicate the proportion of the responses contributed by each of the single cytokines. A key to the colours used for different cytokines in the pie chart arcs is shown.

Figure 3: HIV infection leads to skewing of Th17 response in HIV$^+$IGRA$^+$ chronic progressors but not in long-term non-progressors. PBMCs were cultured overnight in the presence or absence of EC and LT Ag. CD3$^+$CD4$^+$ T-cells were analyzed for intracellular expression of IFN-γ, IL-17A, IL-17F, IL-22 and IL-10. Boolean gates were created from the individual cytokine (listed above) in FlowJo to divide responding cells into 256 distinct subsets corresponding to all possible combinations of these functions and the data was analyzed using COMPASS and SPICE software. All HIV$^+$ subjects were initiated on ART after collection of blood at baseline post diagnosis. (A) Boxplots of data analyzed in COMPASS is shown for the HIV$^-$IGRA$^+$ (N=10, green), HIV$^+$IGRA$^+$ (N=10, red) and HIV$^+$IGRA$^-$ (N=10, blue) groups of probability scores of antigen-specific response for each subject, averaged across selected functional profiles (either IFN-γ$^+$ or IL-10$^+$ cells together with all combinations of IL-17A, IL-17F and IL-22) and across EC or for LT Ag. Probabilities are derived from a COMPASS model fit to ICS data using the Th17 panel. A p-value is shown tested for a difference between groups (two-sided t-test). (B) HIV$^-$IGRA$^+$ (N=10, green) and HIV$^+$IGRA$^+$ (N=10, red) subjects were chosen for comparison of the individual Th17 proinflammatory (IFN-γ$^+$IL-17A$^+$, IFN-γ$^+$IL-17F$^+$, IFN-γ$^+$IL-22$^+$) or regulatory (IL-10$^+$IL-17A$^+$, IL-10$^+$IL-17F$^+$, IL-10$^+$IL-22$^+$) subsets and in (C) HIV$^-$IGRA$^-$ (N=10, brown), HIV$^-$IGRA$^+$ (N=10, green), HIV$^+$IGRA$^-$ (N=10, blue), HIV$^+$IGRA$^+$ (N=10, red), HIV$^+$IGRA$^+$LTNP (N=7, magenta), HIV$^-$TB$^+$ (N=10, black) and HIV$^+$TB$^+$ (N=8, dark grey) subjects were compared for combined double positive Th17 proinflammatory (IFN-γ with IL-17A/IL-17F/IL-22) or regulatory (IL-10 with IL-17A/IL-17F/IL-22) subsets and Tr1 cells (IFN-γ$^+$IL10$^+$) in response to EC or LT Ag pool stimulation. Box-and-whisker plots analyzed by SPICE show the inter-quartile range in absolute numbers with horizontal bar representing the median of (B) individual or (C) combined cellular subsets. Statistical analysis was performed using a one-way ANOVA nonparametric Kruskal–Wallis test and corrected by Dunn's test for multiple comparisons.

Figure 4: ART and ATT modulate CD4+ T effector cytokine responses in HIV$^+$ and TB$^+$ patients. (A) PBMCs from HIV$^+$IGRA$^-$ and HIV$^+$IGRA$^+$ (N=9) patients before ($^-$ART in red) and after treatment ($^+$ART in blue) were stimulated overnight with EC and LT Ag. (B) PBMCs from HIV-TB$^+$ (N=8) patients before ($^-$ATT in red) and after treatment ($^+$ATT in blue) were stimulated overnight with EC and LT Ag. In both (A) and (B), CD3$^+$CD4$^+$ T-cells were analyzed for intracellular expression of IFN-γ, IL-2, MIP-1β, TNF-α, IL-10 and IL-17F in a standard ICS assay. Dots connected with full lines represent matched pairs of patients post

928 treatment ($^{+}$ART or $^{+}$ATT) with treatment naive controls ($^{-}$ART or $^{-}$ATT). Horizontal capped lines represent
929 statistical comparisons between matched patients. Statistical analysis was performed by Wilcoxon
930 matched-pairs signed-rank test with post-hoc Bonferroni's correction for multiple comparisons.
931
932 **Figure 5: ART and ATT restore regulatory Th17 response in HIV-infected and active TB patients**. (A)
933 PBMCs from HIV^{+} subjects (N=9) before (-ART, red) and after 1 year of treatment (+ART, blue) were
934 cultured overnight in the presence or absence of EC and LT Ag. (B) PBMCs from HIV-TB^{+} patients (N=8)
935 before (-ATT, red) and after 6 months treatment (+ATT, blue) were cultured overnight in the presence or
936 absence of EC and LT Ag. In both (A) and (B), CD3^{+}CD4^{+} T-cells were analyzed for expression of IL-17A,
937 IL-17F, IL-22 in combination with IFN-γ or IL-10 using SPICE. Dots connected with full lines represent
938 matched pairs of patients post treatment with treatment naive controls. Horizontal capped lines represent
939 statistical comparisons between matched patients. Statistical analysis was performed using the Wilcoxon
940 matched-pairs signed rank test with post-hoc Bonferroni's correction for multiple comparisons.
941
942 **Figure 6: Comparable cytokine production in activated CD3^{+}CD4^{+}CD45RA^{-}CD154^{+}CD69^{+} cells and**
943 **its un-activated CD3^{+}CD4^{+}CD45RA^{-}CD154^{-}CD69^{-} counterpart in HIV-infected subjects irrespective**
944 **of antigen-specificity.** (A) Schematic overview of flow cytometry-based cell sorting of antigen-specific
945 memory CD4^{+} T-cells for quantification of cell associated HIV DNA, HIV RNA and cytokines. PBMCs from
946 HIV^{+} IGRA^{-} and IGRA^{+} subjects (N=20) were stimulated with EC, LT Ag, HIV-PTE (Gag/Env) pool and CMV
947 for 16 hr. Next, 100 to 250 effector cells were sorted for CD3^{+}CD4^{+}CD45RA^{-}CD154^{+}CD69^{+} and
948 CD3^{+}CD4^{+}CD45RA^{-}CD154^{-}CD69^{-} populations in single cells-to-CT lysis buffer for quantification of cytokine
949 mRNA. Comparison of (B) IFN-γ, (C) IL-2 and (D) MIP-1β gene expression in sorted cells of different
950 antigen specificities. The cDNA was pre-amplified for cytokine mRNA along with GAPDH (reference gene).
951 The fold change of cytokine mRNA is shown in CD154^{+} vs CD154^{-} T-cells which indicates efficient activation
952 of CD3^{+}CD4^{+}CD45RA^{-}CD154^{+}CD69^{+} and not its bystander counterpart CD3^{+}CD4^{+}CD45RA^{-}CD154^{-}CD69^{-}
953 T-cells by various antigens. Statistical analysis was performed using the Wilcoxon matched-pairs signed
954 rank test.
955
956 **Figure 7: Cell-associated HIV DNA and HIV RNA does not significantly vary among cells of different**
957 **antigen specificities.** PBMCs were first blocked with 0.5 µg/ml CD40 (HB14) antibody for 15 min and then

stimulated with anti-CD28/CD49d costimulatory antibody and antigens [EC, LT Ag, CMVpp65 and HIV-PTE (Env-1-3, and Gag 1-2)] pools for 16 hr. Cells were sorted (according to the protocol shown in Figure 6A) to isolate antigen-specific ($CD154^+CD69^+$) and resting ($CD154^-CD69^-$) memory ($CD45RA^-$) $CD4^+$ T-cells, for quantification of cell-associated HIV DNA and HIV RNA. For each subject, 100 to 250 cells were directly sorted into 10µl single cells-to-Ct lysis buffer for RNA extraction whereas remainder cells were collected in 2% RPMI for DNA extraction. (A) HIV DNA copy number was estimated in different Ag-specific $CD154^+CD69^+$ cells. (B) Comparison of HIV DNA copy number in $CD154^+CD69^+$ vs. $CD154^-CD69^-$ cells stimulated with different antigens. (C) Comparative fold change of HIV GAG mRNA in antigen-stimulated $CD154^+CD69^+$ cells relative to its unstimulated control. (D) Comparison of HIV GAG mRNA $CD154^+CD69^+$ vs. $CD154^+CD69^+$ cells upon stimulation with different antigens. Statistical analysis was performed using the Kruskal-Wallis test and Wilcoxon matched-pairs signed rank test.

TABLE 1: Clinical details of study participants.

*M: Male; F: Female

GROUP	N	Sex	AGE (MEDIAN/ RANGE)	CD4 COUNT (MEDIAN/ RANGE)	VIRAL LOAD (MEDIAN/RANGE)
$HIV^{-}IGRA^{-}$	10	M=4; F=6	28 (20-39)	*M: 822 (381-1565)[#] F: 953 (447-1846)	NA
$HIIV^{-}IGRA^{+}$	10	M=8; F=2	30 (25-38)	*M: 822 (381-1565)[#] F: 953 (447-1846)	NA
$HIV^{+}IGRA^{-}$	10	M=7; F=3	31 (24-47)	433.5 (230-721)	37300 (2840-131000)
$HIV^{+}IGRA^{+}$	10	M=5; F=5	37.5 (27-56)	352 (289-540)	27926 (3510-516564)
$HIV^{+}IGRA^{+}$ LTNP[$]	7	M=3; F=4	36.5 (33-48)	823 (679-1259)	9943 (0-19897)
$HIV^{+}IGRA^{+}/IGRA^{-}$ 1Year POST ART	9	M=4; F=5	32 (24-56)	484 (282-524)	Not detected or <40
Pulmonary TB BL & 6 MONTHS POST ATT	5	M=4; F=1	34 (30-66)	*M: 822 (381-1565)[#] F: 953 (447-1846)	NA
Extrapulmonary TB BL & 6 MONTHS POST ATT	3	M=2; F=1	25 (17-45)	*M: 822 (381-1565)[#] F: 953 (447-1846)	NA
HIV-TB	8	M=7; F=1	37 (23-67)	1495 (64-259)	194500 (26200-1160000)

[#] Thakar et al., 2011
[$] Kulkarni et al., 2017

KEY RESOURCES TABLE

REAGENT or RESOURCE	SOURCE	IDENTIFIER
Antibodies		
V450 Mouse Anti-Human IFN-γ	BD Biosciences	Cat# 560371 Clone: B27
FITC Mouse Anti-Human TNF	BD Biosciences	Cat# 552889 Clone: MAb11
Alexa Fluor 700 anti-human IL-2	BioLegend	Cat# 500320 Clone: MQ1-17H12
Brilliant Violet 605 anti-human IL-17A	BioLegend	Cat# 512326 Clone: BL168
Brilliant Violet 650 Mouse Anti-Human IL-17F	BD Biosciences	Cat# 564264 Clone: O33-782
PE-Cy7 Mouse Anti-human IL-22	eBioscience	Cat# 25-7229-42 Clone: 22URTI
Brilliant Violet 786 Rat Anti-Human and ViralIL-10	BD Biosciences	Cat# 564049 Clone: JES3-9D7
PE Mouse Anti-Human MIP-1β	BD Biosciences	Cat# 550078 Clone: D21-1351
APC-H7 Mouse Anti-Human CD45RA	BD Biosciences	Cat# 560674 Clone: HI100
Alexa Fluor 647 anti-human CCR7	BioLegend	Cat# 353218 Clone: G043H7
Brilliant Violet 570 anti-human CD3	BioLegend	Cat# 300436 Clone: UCHT1
BUV395 Mouse Anti-Human CD4	BD Biosciences	Cat# 563550 Clone: SK3
Brilliant Violet 711 Mouse Anti-Human CD8	BD Biosciences	Cat# 563677 Clone: RPA-T8
Alexa Fluor 488 anti-human CD45RA	BioLegend	Cat# 304114 Clone: HI100
PE-Cy7 anti-human CCR7	BioLegend	Cat# 353226 Clone: G043H7
Brilliant Violet 510 anti-human CD14	BioLegend	Cat# 301842 Clone: M5E2
Brilliant Violet 510 anti-human CD19	BioLegend	Cat# 302242 Clone: HIB19
PE Mouse Anti-Human CD154	BD Biosciences	Cat# 555700 Clone: TRAP1
APC Mouse Anti-Human CD69	BD Biosciences	Cat# 340560 Clone: L78
CD40 antibody, Mouse Anti-human	Miltenyi Biotec	Cat# 130-094-133 Clone: HB14
Biological Samples		
PBMC samples from HIV-IGRA-, HIV-IGRA+, HIV+IGRA-, HIV+IGRA+ subjects, Pulmonary and extrapulmonary TB before and after ATT	St. John's Medical College Hospital, Bangalore, India	N/A

PBMC samples from HIV+IGRA+, HIV+IGRA+LTNP individuals	National AIDS Research Institute, Pune, India	N/A
Chemicals, Peptides, and Recombinant Proteins		
Histopaque 1077	Sigma Aldrich	Cat# 10771
Live/Dead Fixable Aqua Dead Cell Stain Kit	Invitrogen	Cat# L34966
ULtraComp eBeads	Invitrogen	Cat# 01-2222-42
Remel Phytohemagglutinin Purified	ThermoFisher Scientific	Cat# R30852801
SuperScript III Reverse Transcriptase	ThermoFisher Scientific	Cat# 18080093
ESAT6/CFP10 fusion protein	Department of Infectious Diseases, Leiden University Medical Center	N/A
Latency antigens (Rv1733c, RV1737c, Rv2029, RV2628)	Department of Infectious Diseases, Leiden University Medical Center	N/A
BD FastImmune CD28/CD49d Purified	BD Biosciences	Cat# 347690, Clone: L293/L25
Brefeldin A Solution (1,000X)	BioLegend	Cat# 420601
Monensin Solution (1,000X)	BioLegend	Cat# 420701
BD FACS Lysing Solution 10X Concentrate	BD Biosciences	Cat# 349202
BD Phosflow™ Perm/Wash Buffer I	BD Biosciences	Cat# 557885
Paraformaldehyde	Electron Microscopy Sciences	Cat# 15712-S
PepMix™ HCMVA (pp65)	JPT Peptide Technologies	Cat# PM-PP65-2
HIV-1 PTE Gag Peptide Pool 1	NIH AIDS Reagent Program	Cat# 12437
HIV-1 PTE-G Env Peptide Pool 1	NIH AIDS Reagent Program	Cat# 12698
Critical Commercial Assays		
TruCOUNT kit	BD Biosciences	Cat# 662415
Abbott RealTime HIV-1 Viral Load Assay	Abbott Molecular Inc.	Cat# 06L18-070

GAPDH Taq Man Gene Expression Assay (Hs99999905_m1)	ThermoFisher Scientific	Cat# 4351370
Taqman gene expression assay IFN-γ (Hs00989291_m1)	ThermoFisher Scientific	Cat# 4331182
Taqman gene expression assay IL-2 (Hs00174114_m1)	ThermoFisher Scientific	Cat# 4331182
Taqman gene expression assay MIP-1β (Hs99999148_m1)	ThermoFisher Scientific	Cat# 4331182
HIV GAG Custom TaqMan Probe Assay ID: AIHSQJI	ThermoFisher Scientific	Cat# 4331348
HIV-1 LTR Vanderg Custom TaqMan® Gene Expression Assay ID: APRWEWY	ThermoFisher Scientific	Cat# 4332078
HUM-CD3-Vanderg Custom TaqMan® Gene Expression Assay ID: APDJXRR	ThermoFisher Scientific	Cat# 4332078
Single Cell-to-CT™ qRT-PCR Kit	ThermoFisher Scientific	Cat# 4458236 & 4458237
Arcturus® PicoPure® DNA Extraction Kit	ThermoFisher Scientific	Cat# KIT0103
TaqMan Gene expression Master Mix	Applied Biosystems	Cat# 4369016
Amplitaq Gold 360 DNA Polymerase	Applied Biosystems	Cat# 4398823
Experimental Models: Cell Lines		
ACH-2 cells	Gift from Dr. Udaykumar Ranga, JNCASR, Bangalore.	Sreenath et al., 2010
HIV (pNL4-3 virus) infected Jurkat T-cells	Gift from Dr. Udaykumar Ranga, JNCASR, Bangalore.	Sreenath et al., 2010
Software and Algorithms		
GraphPad Prism 8.0.2	GraphPad Software	https://www.graphpad.com/
FlowJo version 9.9.6	Becton, Dickinson & Company	https://www.flowjo.com/
FACS DIVA	BD Bioscience	http://www.bdbiosciences.com/

COMPASS	Lin L et al. Nat Biotechnol. 2015; 33(6):610–616	www.bioconductor.org › bioc › COMPASS › inst › doc
Pestle v1.8	Roederer M et al. Cytometry A. 2011;79(2):167–174.	https://niaid.github.io/spice/
SPICE v5.1	Roederer M et al. Cytometry A. 2011;79(2):167–174.	https://niaid.github.io/spice/
7000 System SDS Software v1.2.3	Applied Biosystems	https://resource.thermofisher.com/pages 2013/WE111944/

Figure

Click here to access/download;Figure;CR_Figure 1.tif

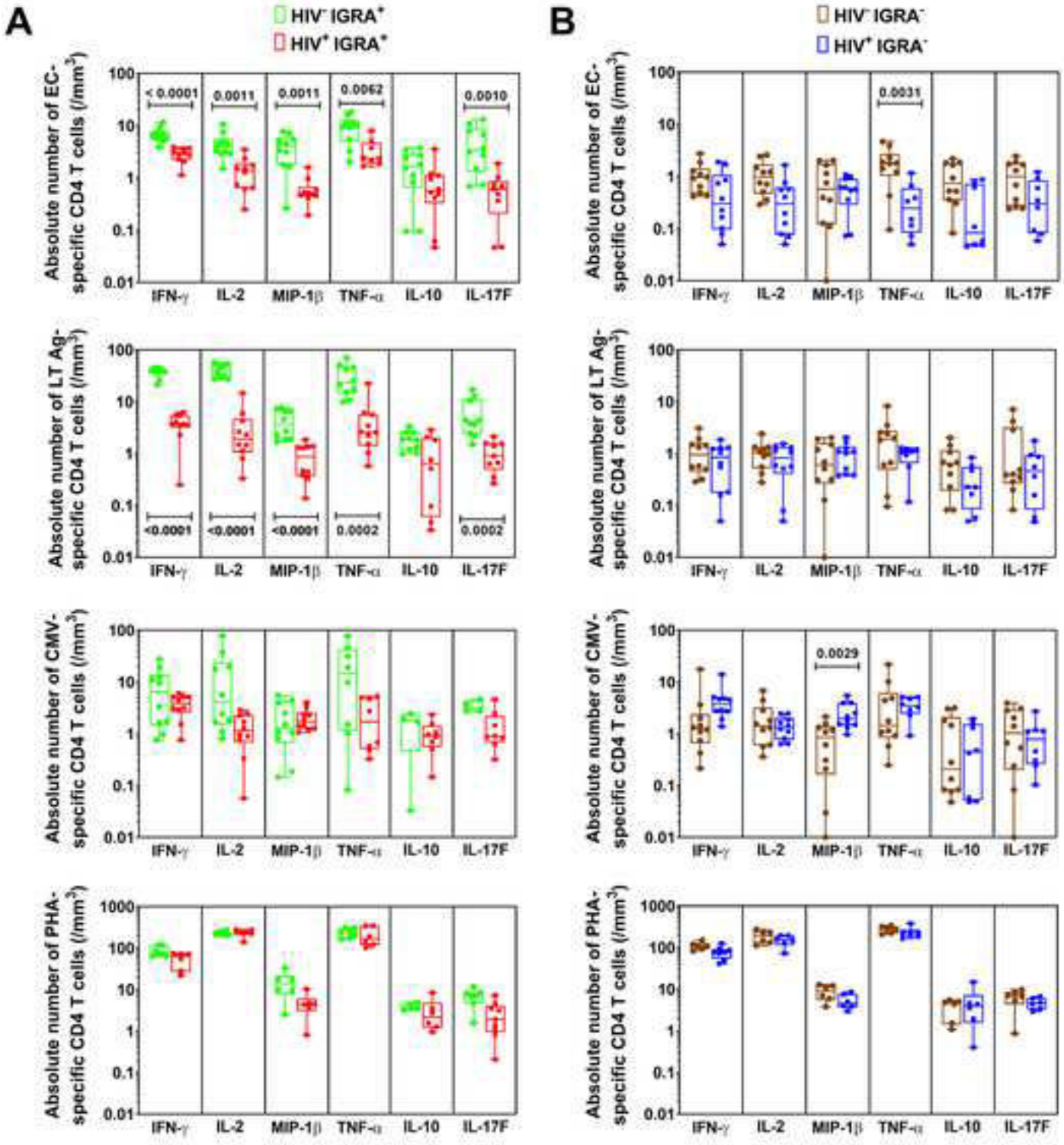

Figure

Click here to access/download;Figure;CR_Figure 2.tif

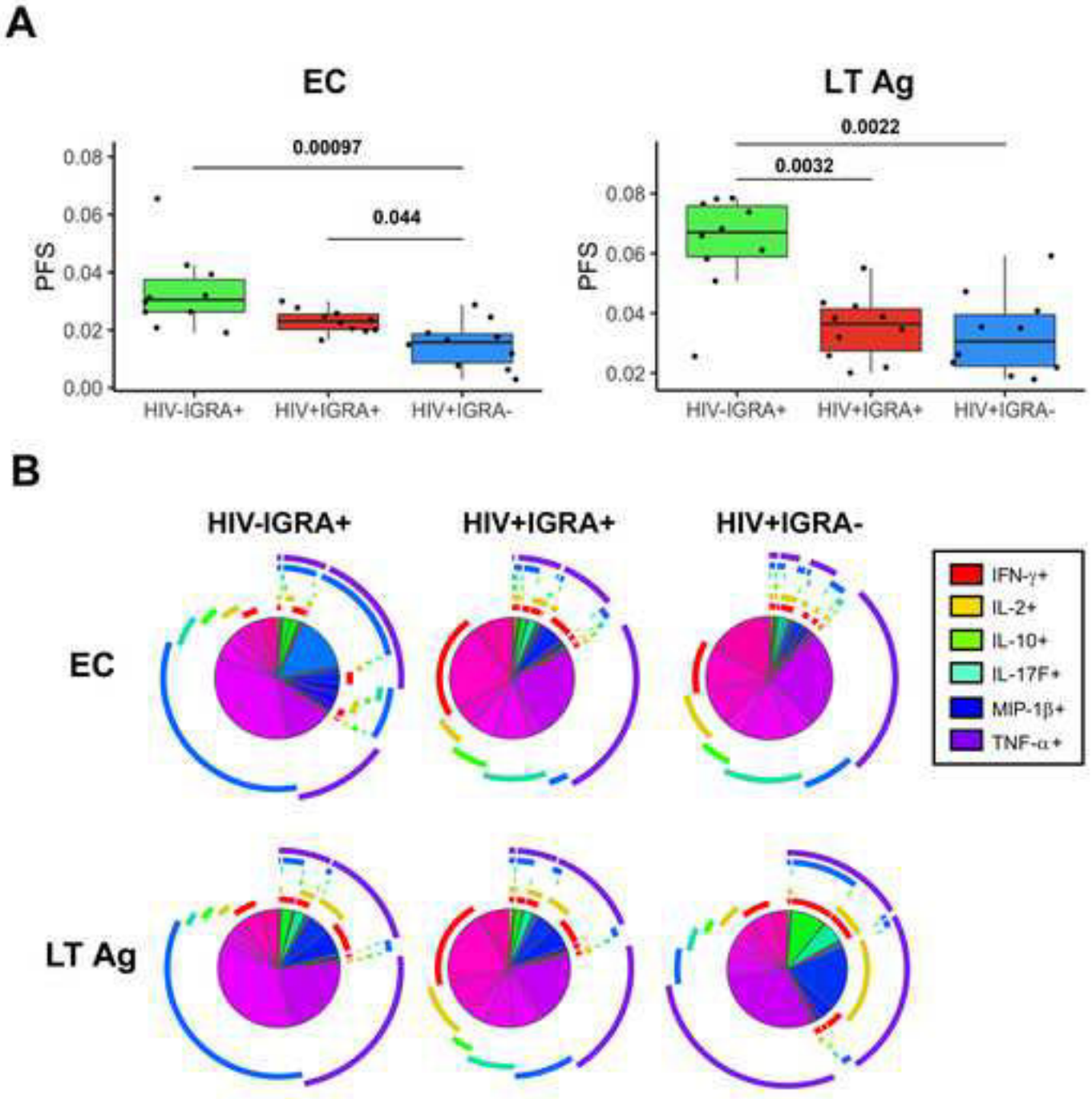

Figure

Click here to access/download;Figure;CR_Figure 3.tif

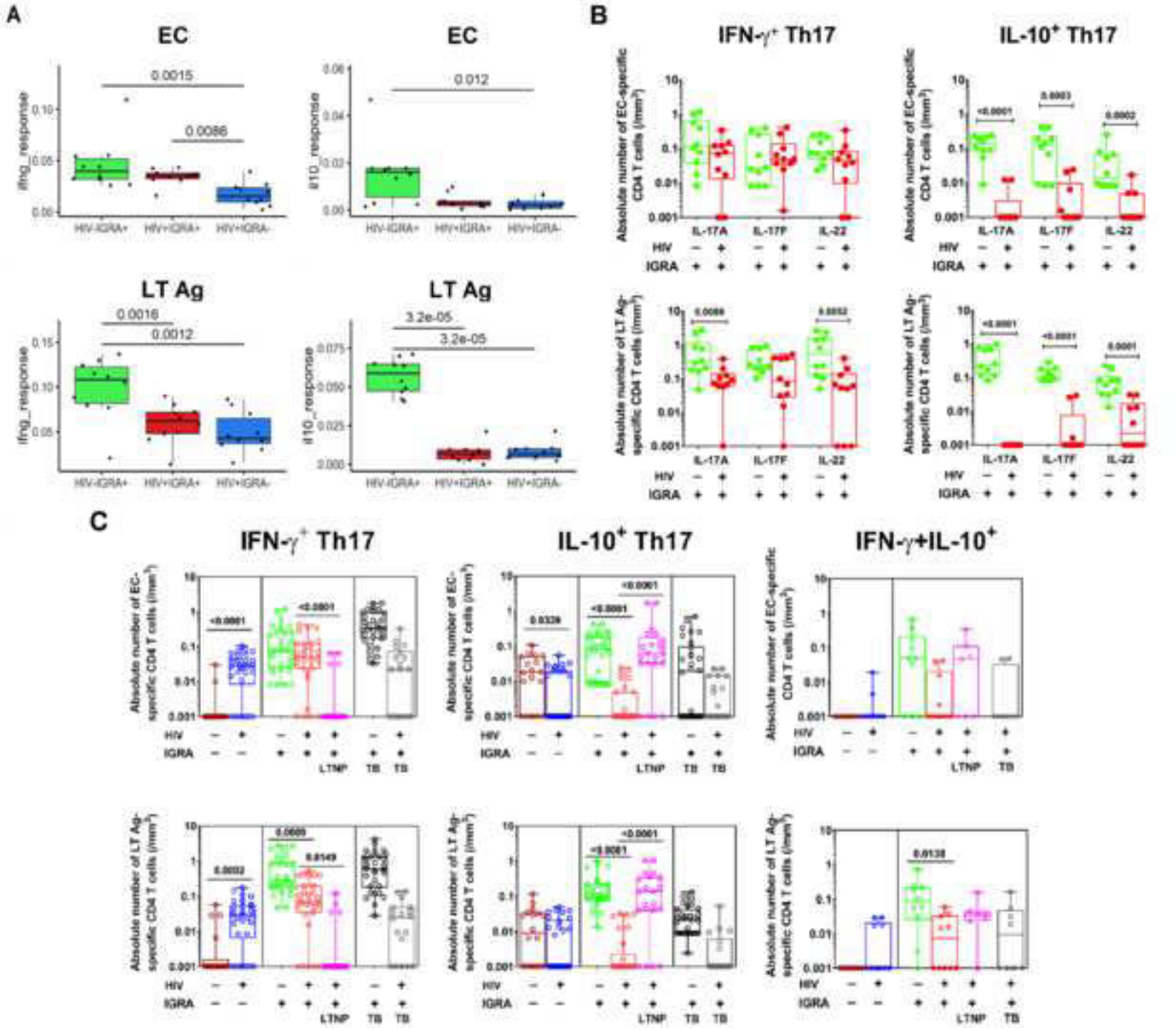

Figure

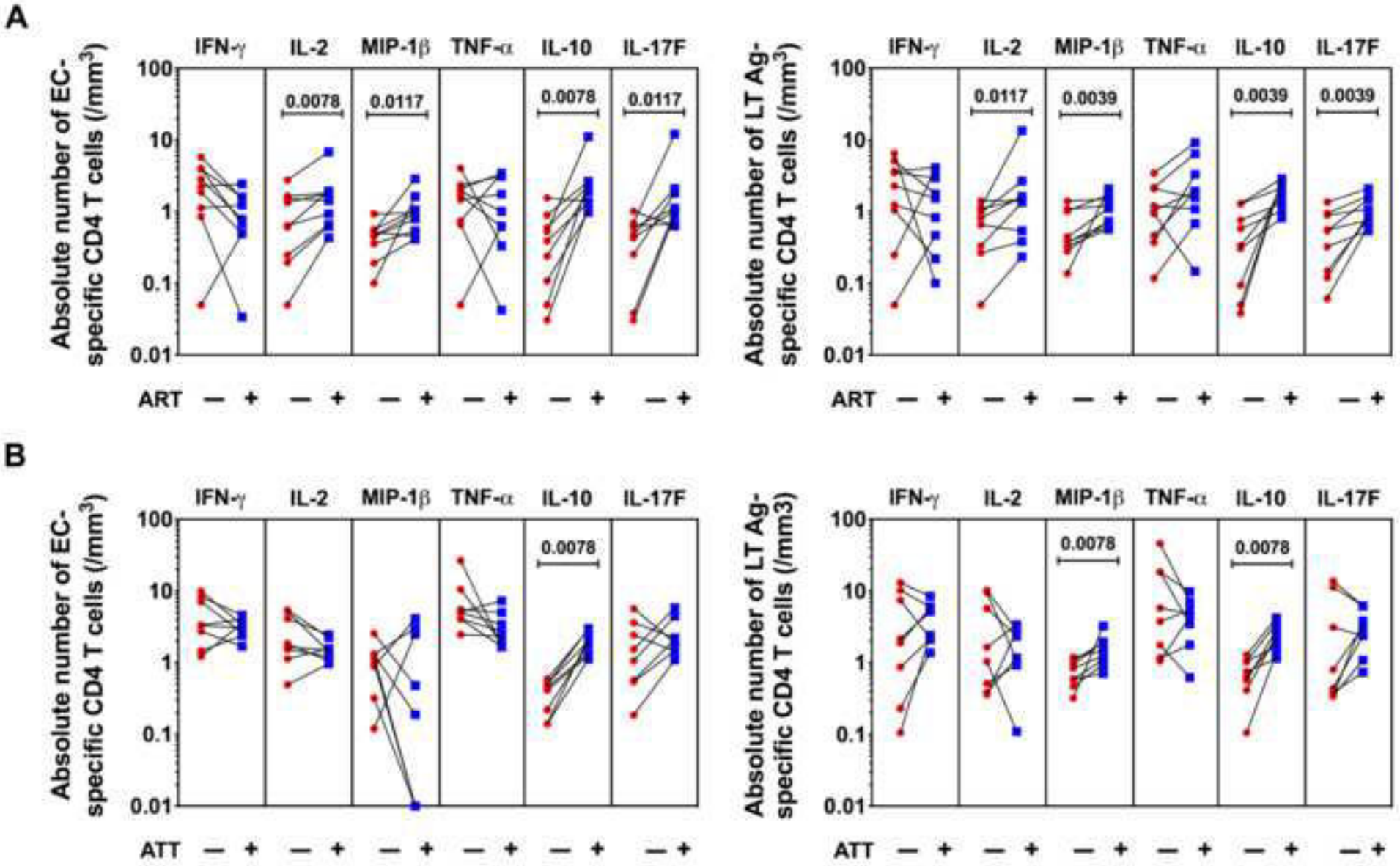

Figure

Click here to access/download;Figure;CR_Figure 5.tif

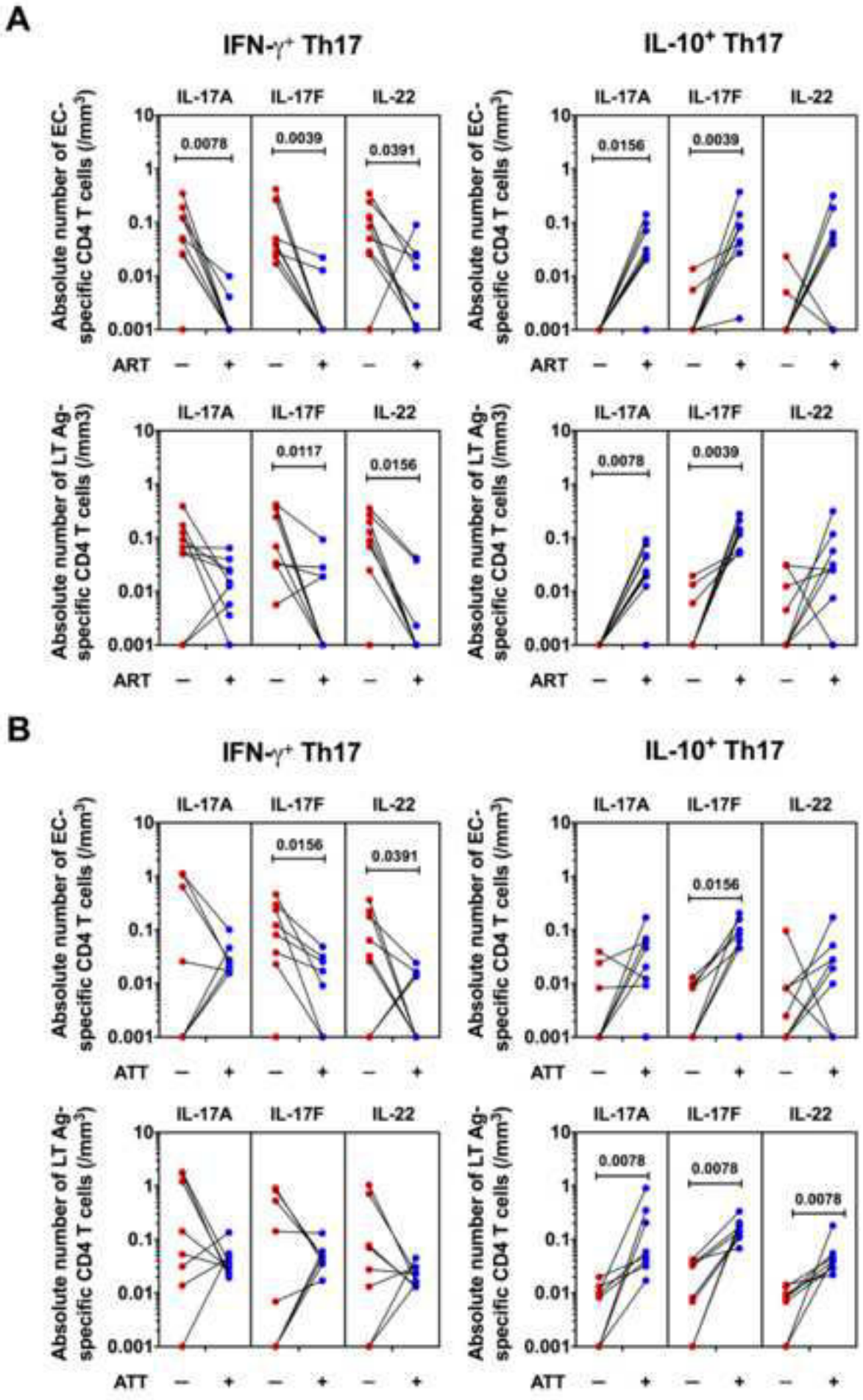

Figure

Click here to access/download;Figure;CR_Figure 6.tif

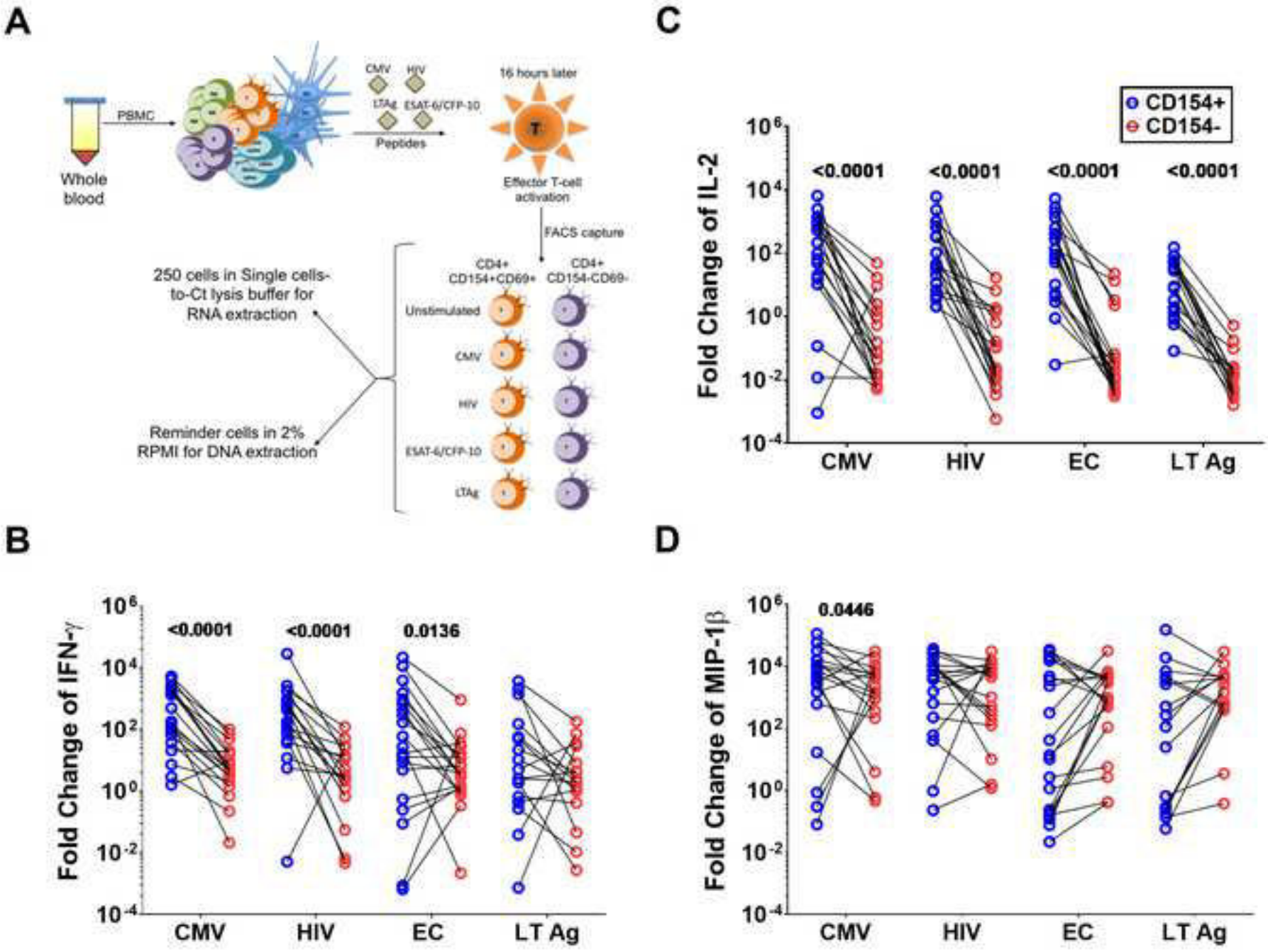

Figure

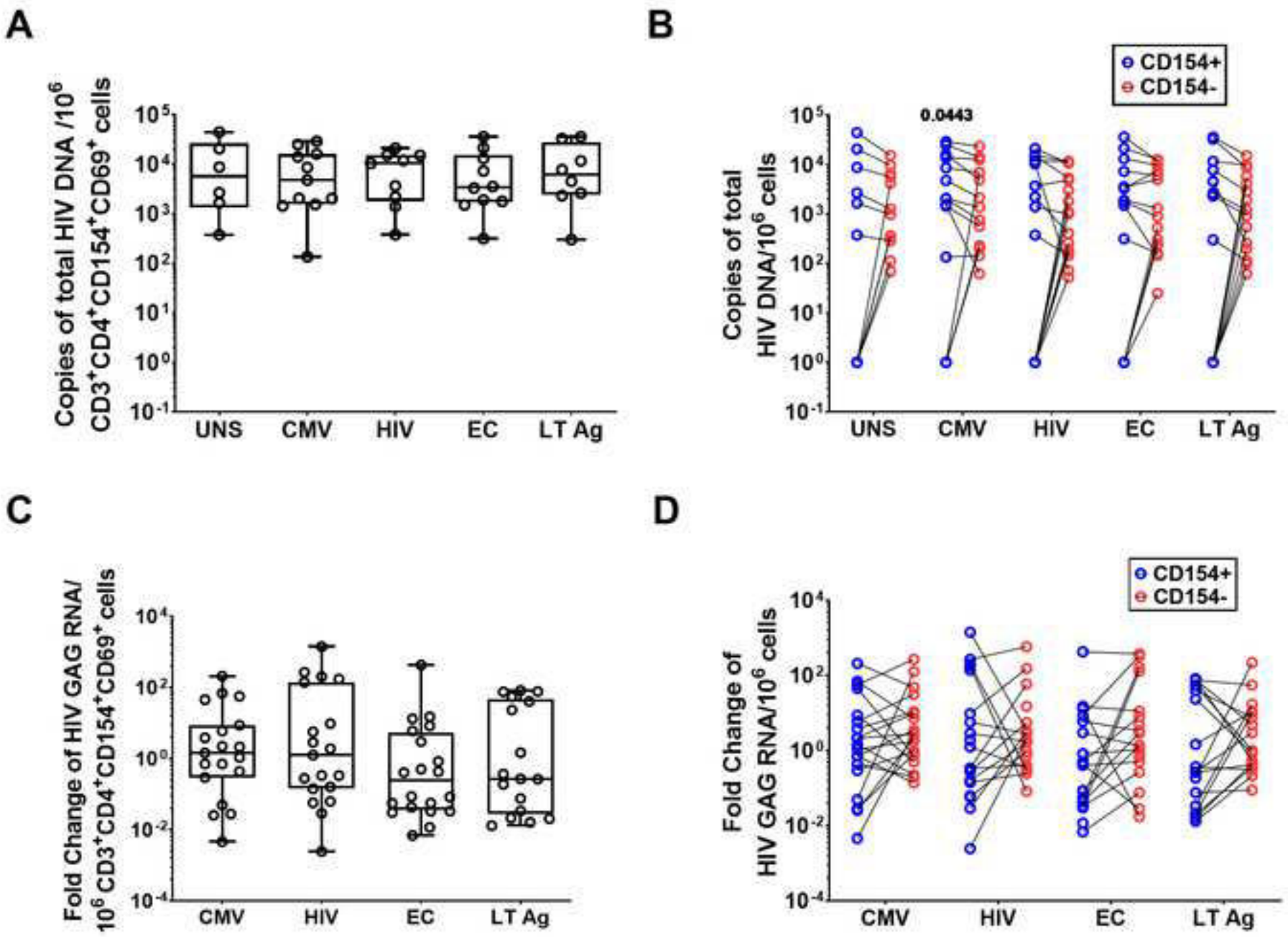

Supplemental Information

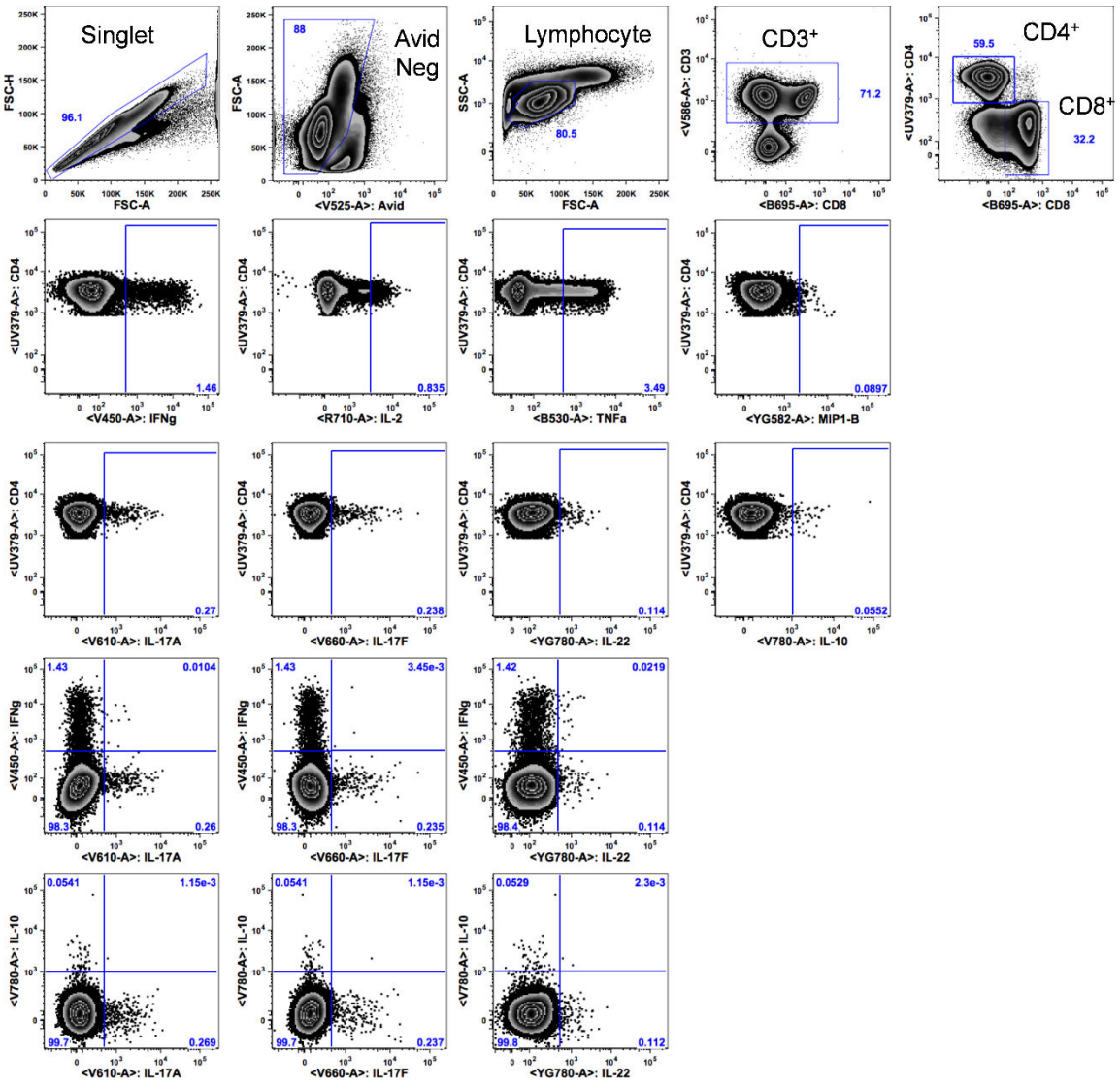

Figure S1: Schematic representation of flow cytometry data and sequential gating strategy used to detect cytokine production by CD4⁺ T cells in a HIV⁺IGRA⁺ subject upon EC stimulation. Initial gating was done on FSC-H and FSC-A to discriminate singlets, followed by the exclusion of dead cells by AVID stain. Lymphocytes were gated using FSC-A and SSC-A. Within the lymphocyte gate, CD3⁺ cells were first identified, followed by CD4⁺ and CD8⁺ T cells. To define functional markers for CD4⁺ T cells, a gate was applied for each cytokine, not taking into account the co-expression of other markers. All gates for non-functional markers were defined using fluorescence minus one (FMO) controls; gates for functional markers were defined using the unstimulated samples. CD4⁺ T cells expressing Th17 cytokines in combination with IL-10 or IFN-γ are also shown by quadrant gating. Boolean gates were then created based on these gates to identify cells expressing different combination of markers.

A

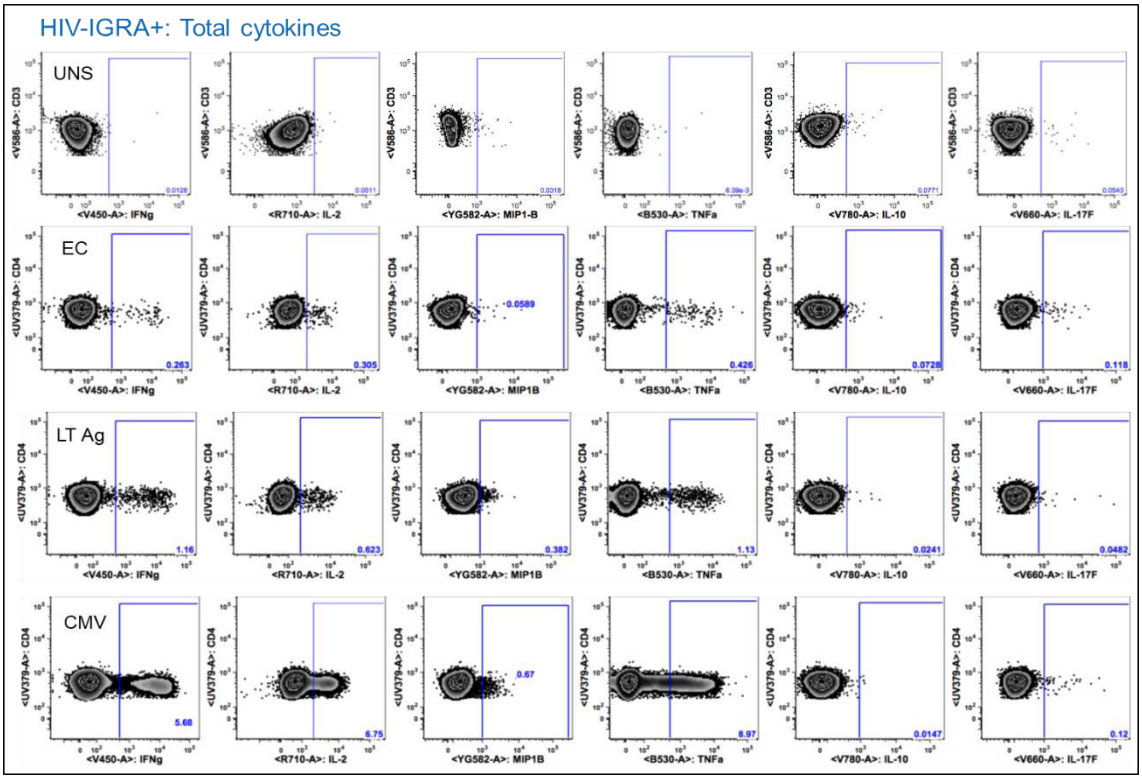
HIV-IGRA+: Total cytokines
UNS
EC
LT Ag
CMV
<V586-A>: CD3
<UV379-A>: CD4
<V450-A>: IFNg
<R710-A>: IL-2
<YG582-A>: MIP1-B
<B530-A>: TNFa
<V780-A>: IL-10
<V660-A>: IL-17F

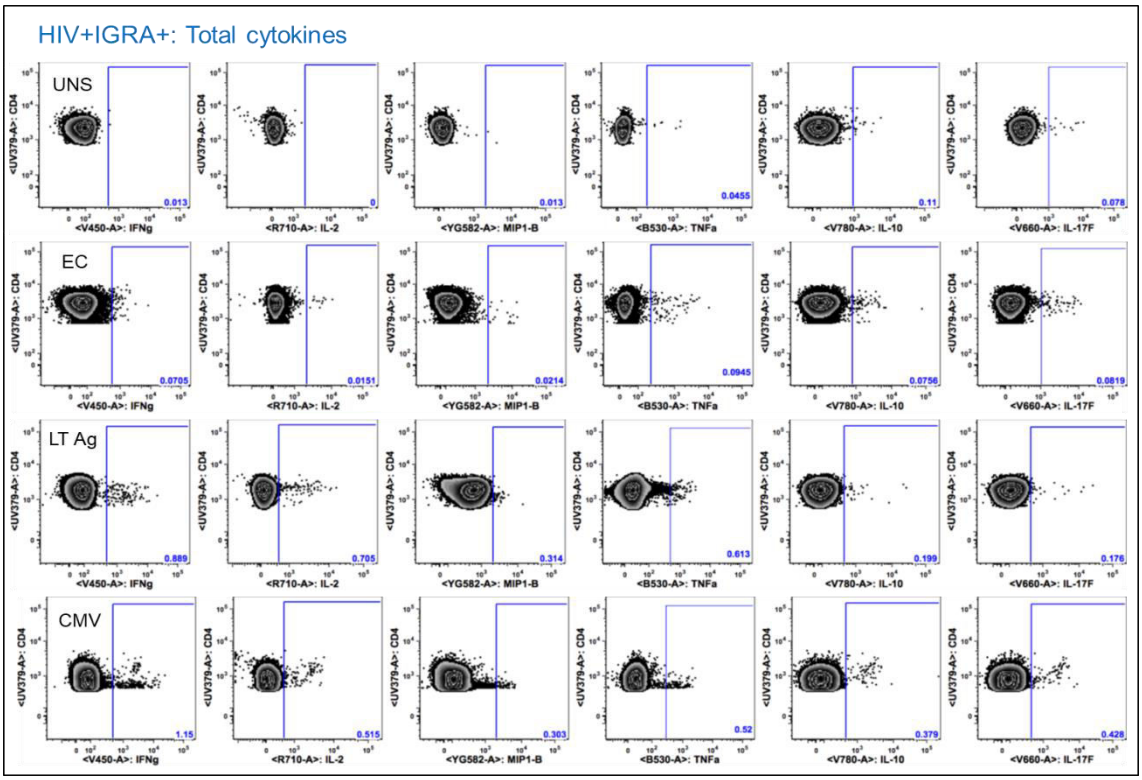
HIV+IGRA+: Total cytokines
UNS
EC
LT Ag
CMV
<UV379-A>: CD4
<V450-A>: IFNg
<R710-A>: IL-2
<YG582-A>: MIP1-B
<B530-A>: TNFa
<V780-A>: IL-10
<V660-A>: IL-17F

B

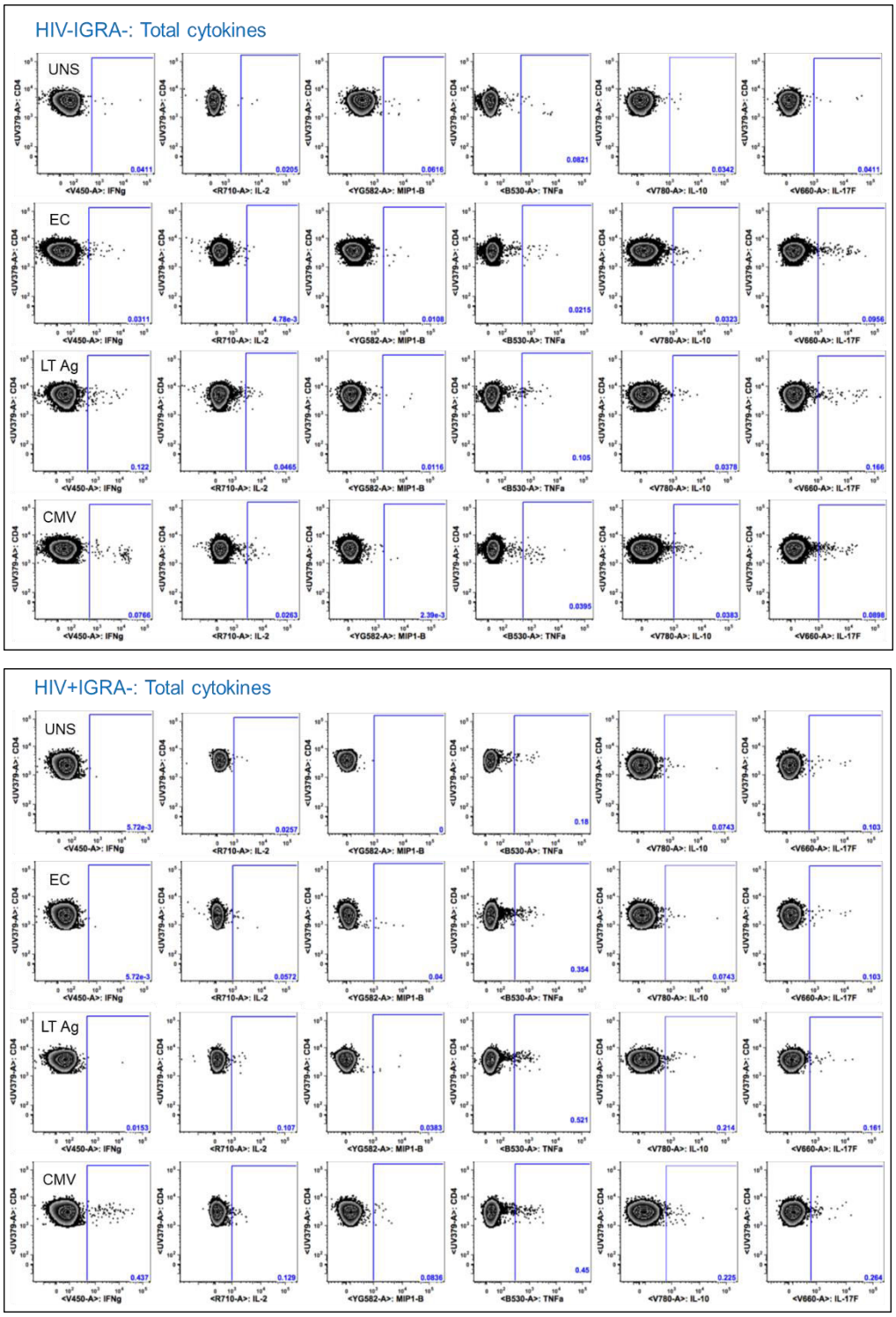

Figure S2: Expression of effector cytokines by CD4⁺ T cells in the four clinical groups. PBMCs were stimulated overnight with EC (10µg/ml), LT Ag (10µg/ml) and CMVpp65 (1.7µg/ml). $CD3^+CD4^+$ T-cells were analysed for intracellular expression of IFN-γ, IL-2, MIP-1β, TNF-α, IL-10 and IL-17F in a standard ICS assay. Representative FACS plots gated on $CD4^+$ T cells showing cytokine expression from (A) HIV^-IGRA^+ vs. HIV^+IGRA^+ and (B) HIV^-IGRA^- vs. HIV^+IGRA^- subjects in absence of stimulation (UNS) and in response to EC, LT Ag and CMV stimulation. The values (in blue) within the gates indicate the frequencies of cytokine-producing total $CD4^+$ T-cells.

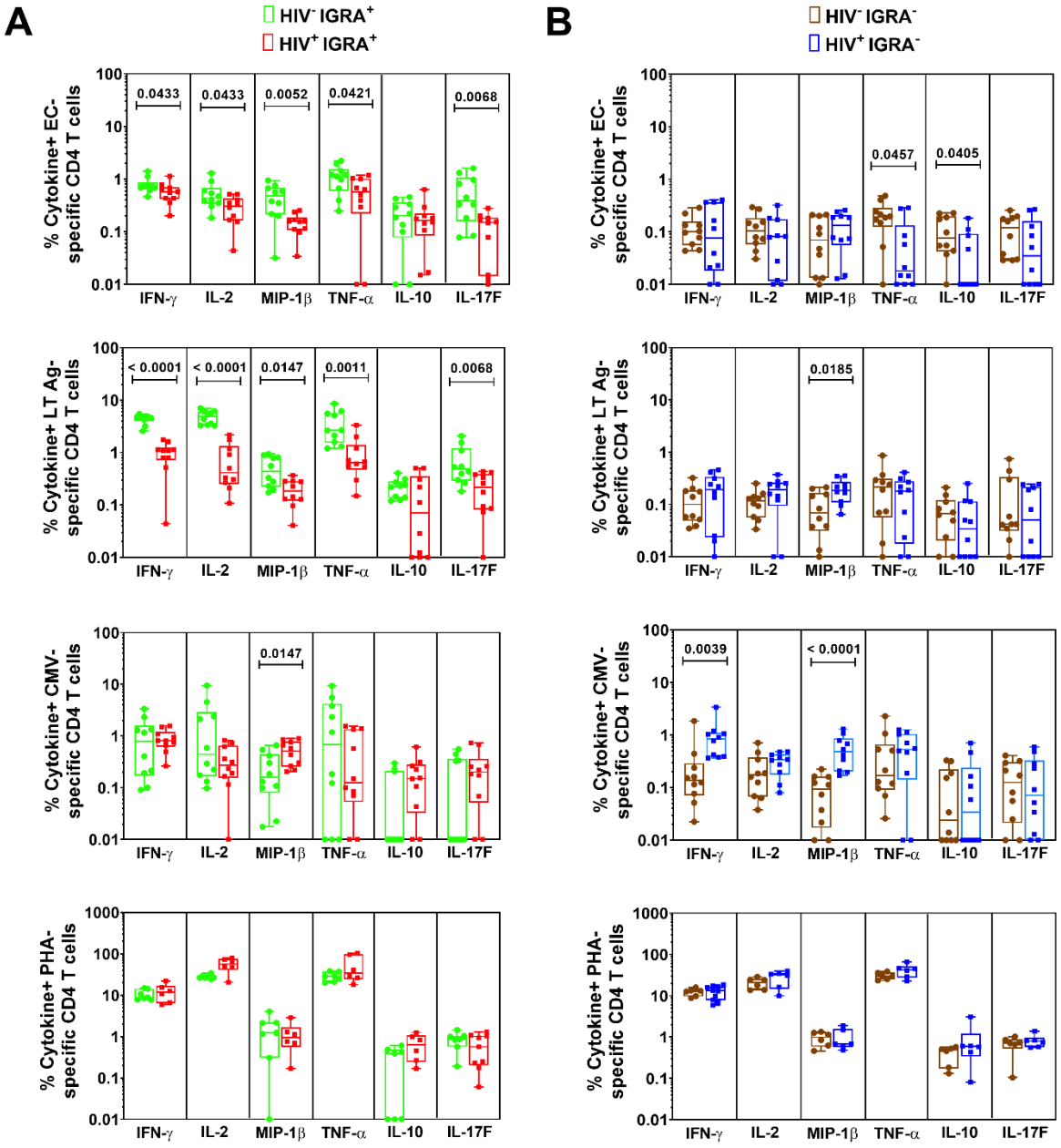

Figure S3: HIV infection modulates the expression of effector cytokines in Mtb-specific CD4⁺ T-cells. PBMCs from (A) HIV⁻IGRA⁺ (N=10, green) vs. HIV⁺IGRA⁺ (N=10, red) and (B) HIV⁻IGRA⁻ (N=10, brown) vs. HIV⁺IGRA⁻ (N=10, blue) subjects were stimulated overnight with ESAT6/CFP10 (10µg/ml), LT Ag pool (10µg/ml), CMVpp65 (1.7µg/ml) and PHA (1µg/ml). CD3⁺CD4⁺ T-cells were analysed for intracellular expression of IFN-γ, IL-2, MIP-1β, TNF-α, IL-10 and IL-17F in a standard ICS assay. Frequencies of cytokine-producing total CD4⁺ T-cells were obtained after background subtraction of values from unstimulated control. Box-and-whisker plots show the inter-quartile range and horizontal bars represent the median frequencies of total cytokine-positive CD4⁺ T-cells. Statistical analysis was performed by Mann-Whitney t test with Bonferroni's correction for multiple comparisons

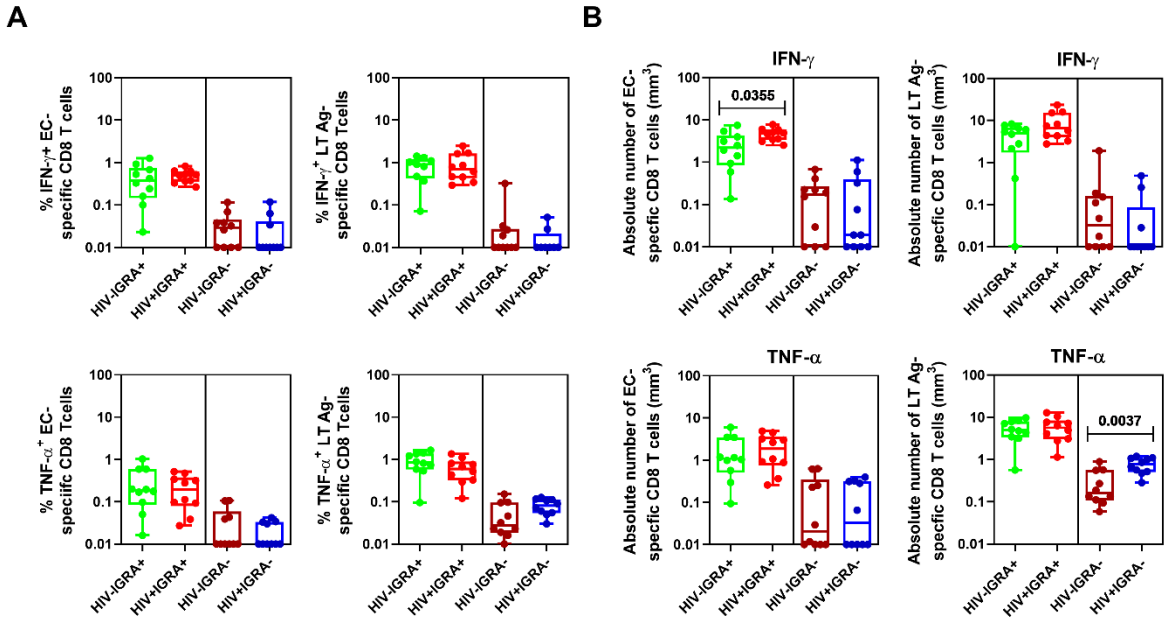

Figure S4: HIV infection does not significantly modulate the expression of effector cytokines in Mtb-specific CD8⁺ T-cells. PBMCs from HIV⁻IGRA⁺ (N=10, green) vs. HIV⁺IGRA⁺ (N=10, red) and HIV⁻IGRA⁻ (N=10, brown) vs. HIV⁺IGRA⁻ (N=10, blue) subjects were stimulated overnight with ESAT6/CFP10 (10µg/ml) and LT Ag pool (10µg/ml). CD3⁺CD8⁺ T-cells were analysed for intracellular expression of IFN-γ and TNF-α in a standard ICS assay. (A) Frequencies of cytokine-producing total CD8⁺ T-cells were obtained after background subtraction of values from unstimulated control. (B) Absolute numbers of antigen-specific CD8⁺ T cells were calculated by multiplying the frequencies of cytokine-positive CD8⁺ T cells by the total CD8⁺ T-cell count. Box-and-whisker plots show the inter-quartile range and horizontal bars represent the median frequencies or absolute numbers of total cytokine-positive CD8⁺ T-cells. Statistical analysis was performed by Mann-Whitney test with Bonferroni's correction for multiple comparisons.

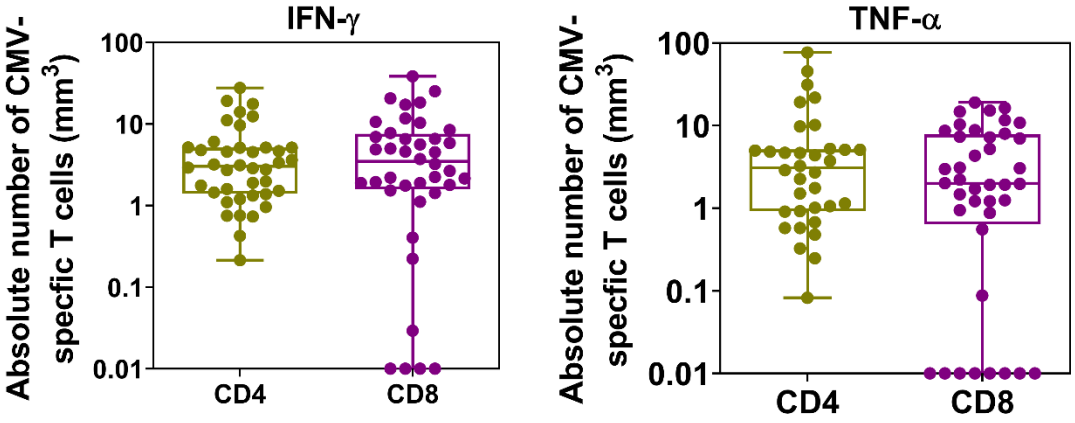

Figure S5: CMV-specific responses in HIV-uninfected and HIV-infected individuals. PBMCs from HIV$^-$IGRA$^+$, HIV$^+$IGRA$^+$, HIV$^-$IGRA$^-$ and HIV$^+$IGRA$^-$ (N=40) subjects were stimulated overnight with CMV (1.7µg/ml). CD3$^+$CD4$^+$ and CD3$^+$CD8$^+$ T-cells were analysed for intracellular expression of IFN-γ and TNF-α in a standard ICS assay. Absolute numbers of antigen-specific CD4$^+$ and CD8$^+$ T cells were calculated by multiplying the frequencies of cytokine-positive CD4$^+$ and CD8$^+$ T cells by the total CD4$^+$ and CD8$^+$ T-cell count respectively. Box-and-whisker plots show the inter-quartile range and horizontal bars represent the median absolute numbers of total cytokine-positive CD4$^+$ and CD8$^+$ T-cells.

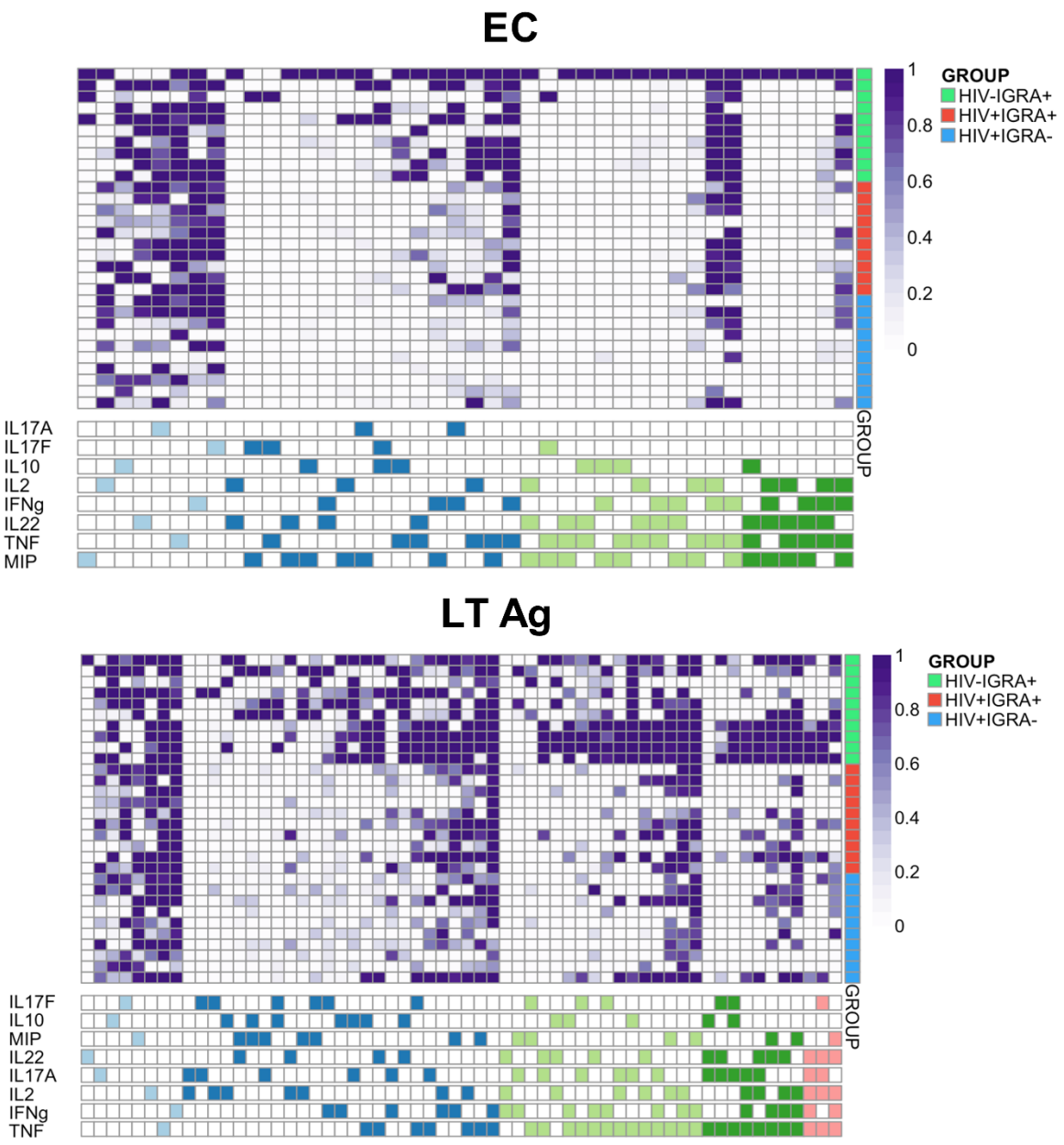

Figure S6: HIV infection dramatically impacts the polyfunctional response. Stacked COMPASS heat maps displaying CD4⁺ T cell responses to EC and LT Ag in three clinical groups. In the heat map, columns correspond to the different disjoint cell subsets in which responses were detected and are color-coded by the cytokines they express (white = "off", shaded = "on", grouped by colour = "degree of functionality"), and are displayed in order of increasing functionality from left to right i.e. sky blue representing one cytokine to peach representing combinations of 5 cytokines. For example, the first column represents CD4⁺ T cells that produce MIP-1β but none of the other functions. Rows represent study subjects (N = 10 per group), which are ordered by their infection status: HIV⁻IGRA⁺ (top, green), HIV⁺IGRA⁻ (middle, pink) and HIV⁺IGRA⁺ (bottom, blue), and by PFS within each group. Each cell of the heatmap shows the probability estimated by COMPASS that the observed response is antigen-specific in the corresponding subject (row) and cell subset (column), where the probability is color-coded from white (zero) to purple (one). A probability of 0 indicates certainty that the observed response is background, while a probability of 1 indicates certainty that the observed response is antigen-specific.

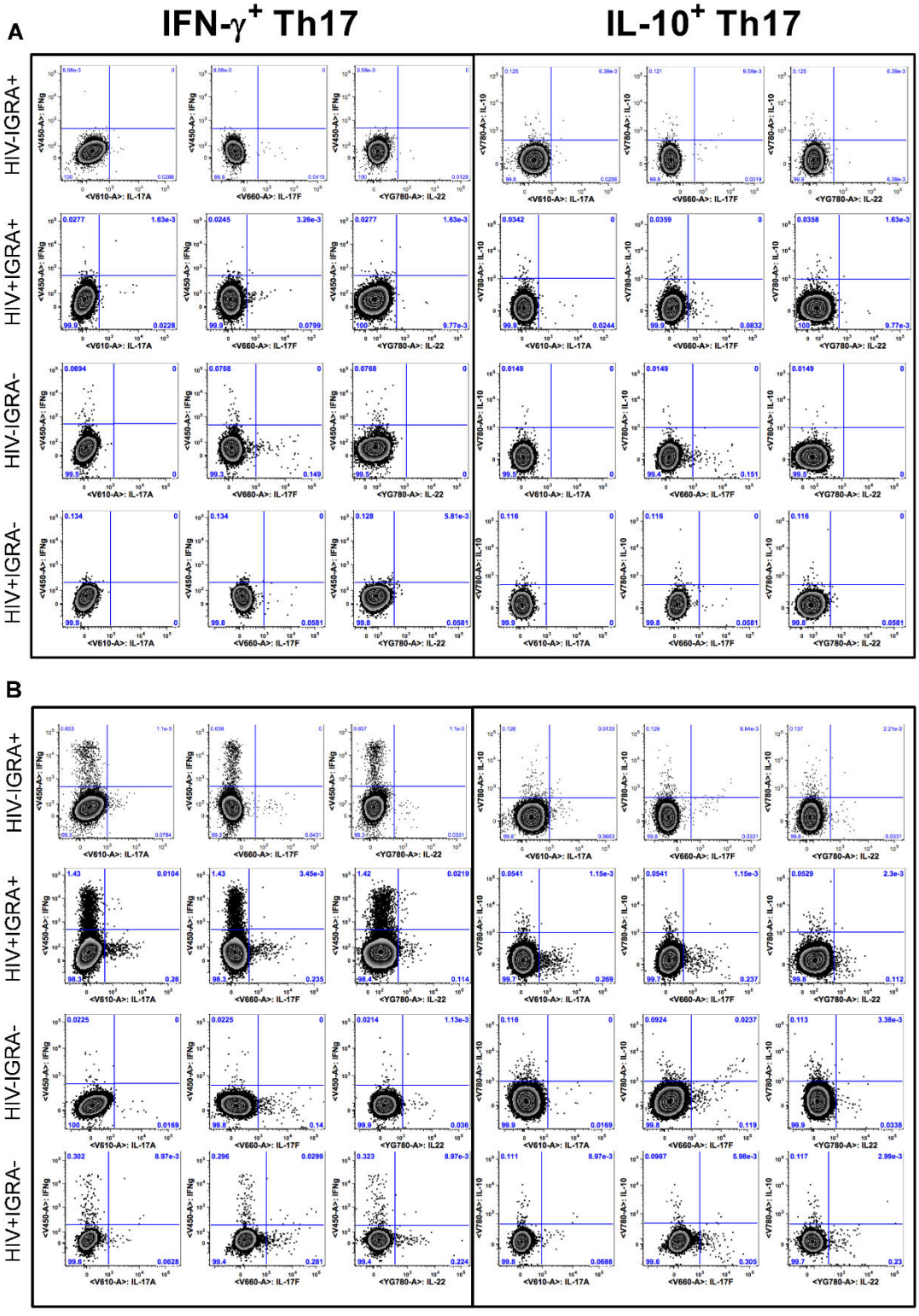

Figure S7: Gating strategy for Th17 subsets in HIV uninfected and infected IGRA$^+$ and IGRA$^-$ subjects. Representative FACS plots gated on CD4$^+$ T cells showing the proinflammatory IFN-γ$^+$Th17 (IFN-γ with IL-17A/IL-17F/IL-22) and regulatory IL-10$^+$ Th17 (IL-10 with IL-17A/IL-17F/IL-22) subsets in IGRA$^-$ and IGRA$^+$ subjects with and without HIV infection in the (A) absence or (B) presence of LT Ag stimulation.

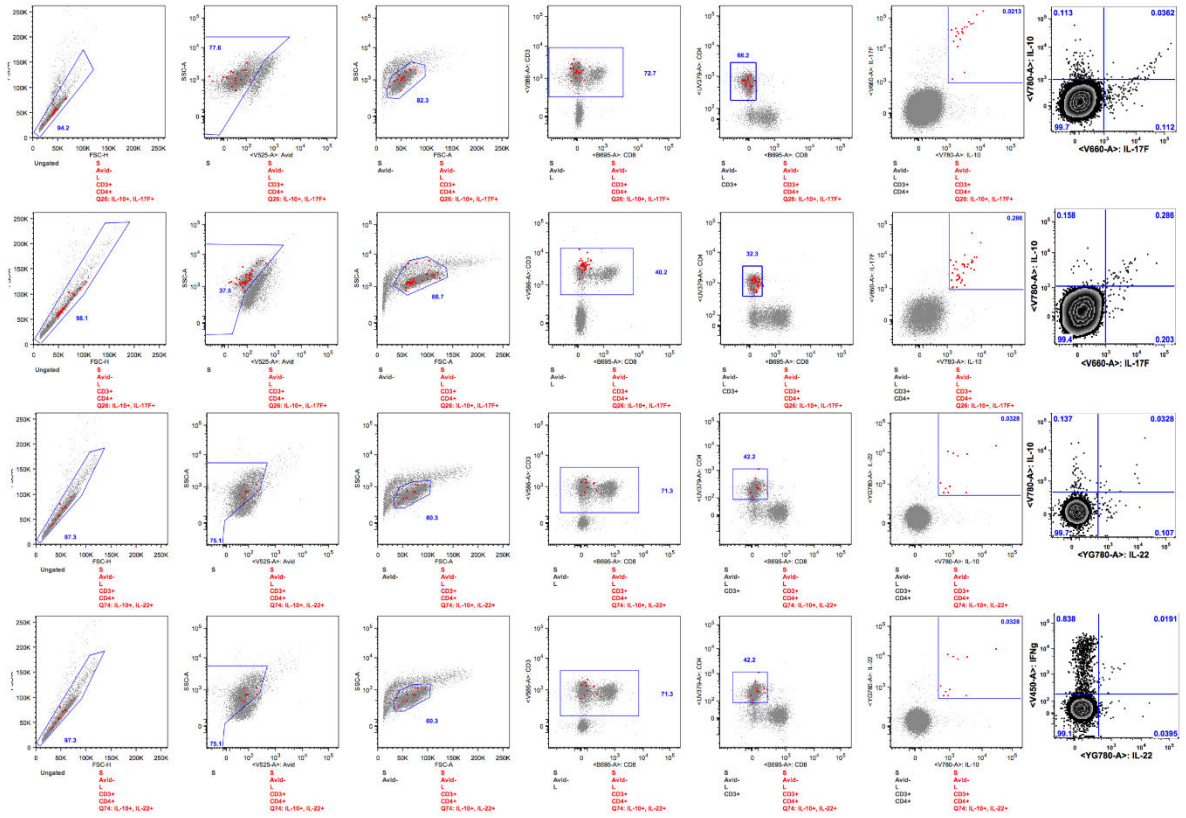

Figure S8: Backgating to show IL-10^{+} Th17 and IFN-γ^{+} Th17 cells that represent minor but viable cell populations and lie within the region gates.

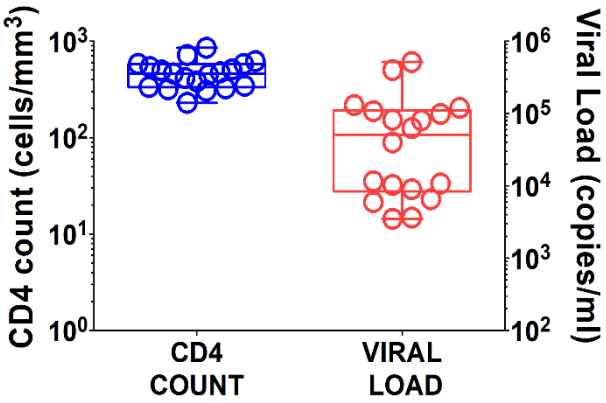

Figure S9: Comparison of CD4 T cell count (cells/mm^3) vs. viral load (copies/ml) in HIV infected IGRA$^-$ and IGRA$^+$ patients.

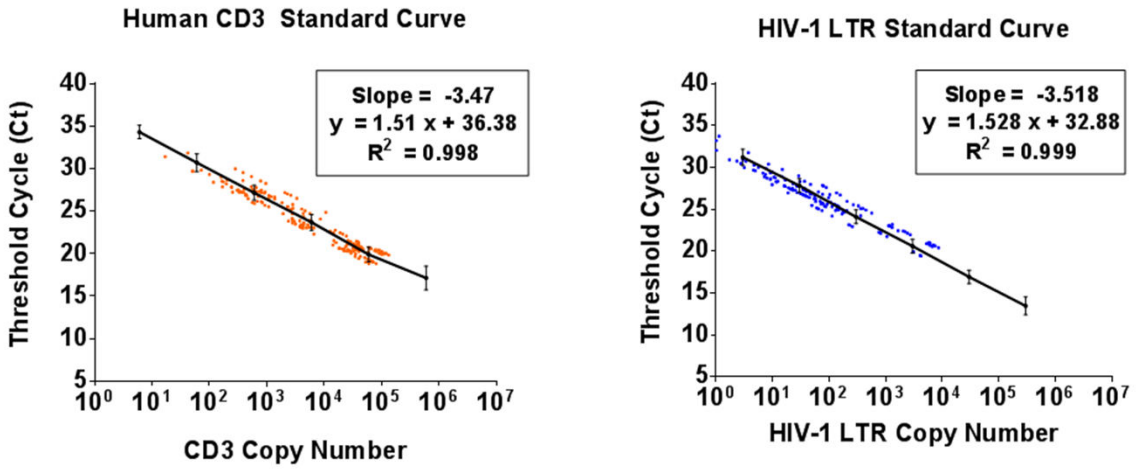

Figure S10: Human CD3 and HIV-1 LTR standard curves for quantification of cell-associated HIV DNA in sorted Ag-specific CD4 T cells of HIV-infected subjects. Standard curves were generated using 10-fold serial dilution series of ACH-2 cellular DNA for both HIV-1 LTR and Human CD3 gene in each of the 11 different experiments. LTR and CD3 copy numbers were calculated from the respective standard curves of each individual experiment and total cell associated HIV DNA copies per million $CD4^+$ T-cells were determined by calculating the number of cells from the human CD3 gene copy number which is present as 2 copies of CD3 gene per cell. Mean standard curves for human CD3 gene and HIV-1 LTR gene generated from 11 experiments are shown.

Results for Figure S6

Heatmaps of cell-subset response probabilities in all subjects from three clinical groups (HIV^-IGRA^+, HIV^+IGRA^+ and HIV^-IGRA^-) studied for EC- and LT Ag-specific $CD4^+$ T-cell responses were generated by COMPASS analysis (**Figure S6)**. We observed that single-positive cells expressing IFN-γ, TNF-α and Th17 (IL-17A, IL-17F and IL-22) cytokines mostly remained unchanged, with an increase only in $IL\text{-}2^+$ cells; however, MIP-1β and IL-10 single-positive cells were drastically reduced in HIV^+IGRA^+ compared to HIV^-IGRA^+ subjects in response to EC stimulation. $CD4^+$ subsets expressing TNF-α in combination with IL-2, MIP-1β, IL-10 or IL-22 as well as $IL\text{-}10^+IL\text{-}17F^+$ were markedly reduced in HIV^+IGRA^+ vs. HIV^-IGRA^+ subjects. We also observed a slight decrease of 4^+ ($IFN\text{-}\gamma^+IL\text{-}2^+TNF\text{-}\alpha^+MIP\text{-}1\beta^+$) $CD4^+$ T-cell subset, however, no significant changes were observed in the probability of 3^+ subset ($IFN\text{-}\gamma^+IL\text{-}2^+TNF\text{-}\alpha^+$) between the HIV^-IGRA^+ and HIV^+IGRA^+ subjects (**Figure S6**). Interestingly, there was a profound impairment in the polyfunctional response to LT Ag stimulation compared to EC, with HIV-infected $IGRA^+$ subjects having relatively smaller proportion of cells that express a combination of 2, 3, 4 and 5 cytokines, compared with HIV-uninfected $IGRA^+$ subjects. The analysis also revealed that $IFN\text{-}\gamma^+IL\text{-}2^+$ as well as dual subsets producing MIP-1β or IL-10 in combination with Th17 cytokines to be most significantly reduced. Within subsets that expressed 3, 4, or 5 cytokines, HIV infection considerably decreased subsets that predominantly expressed TNF-α and/or Th17 cytokines in combination with IL-10, although the probability of $IFN\text{-}\gamma^+IL\text{-}2^+TNF\text{-}\alpha^+$ subset remained unchanged. No significant differences between HIV-infected and HIV-uninfected individuals were detected in the proportions of single-positive $CD4^+$ T-cells except for $IL\text{-}10^+$ and $MIP\text{-}1\beta^+$ (**Figure S6**).

Click here to access/download

Supplemental File Sets

CR_Supplemental Clinical File_14 Sep 20.xlsx